Modeling the spatial dynamics of marsh ponds in New England salt marshes

G. Mariotti[1,2], A.C. Spivak[3], S.Y. Luk[4], G. Ceccherini[5], M. Tyrrell[6], M. Eagle Gonneea[7]

1. Louisiana State University, Department of Oceanography and Coastal Sciences, Baton Rouge (LA), USA
2. Louisiana State University, Center for Computation and Technology, Baton Rouge (LA), USA
3. University of Georgia, Department of Marine Sciences, Athens (GA), USA
4. Woods Hole Oceanographic Institution, Department of Marine Chemistry and Geochemistry, Woods Hole (MA), USA
5. Joint Research Centre, Bioeconomy Unit, European Commission, Ispra, Italy
6. Waquoit Bay National Estuarine Research Reserve, Falmouth (MA), USA
7. U.S. Geological Survey, Woods Hole (MA), USA

Abstract

Ponds are common features on salt marshes, yet it is unclear how they affect large-scale marsh evolution. We developed a spatially explicit model that combines cellular automata for pond formation, expansion, and drainage, and partial differential equations for elevation dynamics. We use the mesotidal Barnstable marsh (MA, USA) as a case study, for which we measured pond expansion rate by remote sensing analysis over a 41-year time span. We estimated pond formation rate by comparing observed and modeled pond size distribution, and predicted pond deepening by comparing modeled and measured pond depth. The Barnstable marsh is currently in the pond recovery regime, i.e., every pond revegetates and recovers the necessary elevation to support plant growth after re-connecting to the channel network. This pond dynamic creates an equivalent (i.e., spatially and temporally averaged over the whole marsh) 0.5-2 mm/yr elevation

loss that needs to be supplemented by excess vertical accretion. We explore how the pond regime would change with decreased sediment supply and increased relative sea-level rise (RSLR) rate, focusing on the case in which the vegetated marsh keeps pace with RSLR. When the RSLR rate remains below the minimum unvegetated deposition rate, the pond dynamics is nearly unaltered and ponds always occupy ~10% of the marsh area. However, when RSLR rate exceeds this threshold, the ponds in the marsh interior – which receive the least amount of suspended sediment – do not recover after drainage. These ponds transition to mudflats and permanently occupy up to 30% of the marsh area depending on RSLR rate. For marshes with a small tidal range, such as the microtidal Sage Lot Pond marsh on the opposite side of the peninsula from Barnstable marsh, high RSLR rates could bring every portion of the marsh into the pond runaway regime, with the whole marsh eventually converting into mudflats. In this regime, the existing marsh would disappear within centuries to millennia depending on the RSLR rate. Because of the spatial and temporal components of marsh evolution, a single RSLR threshold value applied across the entire marsh landscape provides a limited description of the marsh vulnerability to RSLR.

1. Introduction

Marsh evolution models commonly assume a homogenous marsh platform, in which both elevation and plant biomass change smoothly except close to a few ecotones (Marani et al., 2013). On the contrary, many marsh platforms are highly heterogeneous because of the presence of ponds – semicircular depressions permanently inundated even at low tide. This heterogeneity is particularly relevant for the Mid-Atlantic and New England coast of the USA, where ponds are ubiquitous features (Harshberger, 1909; Redfield, 1972; Adamowicz and Roman, 2005; Schepers et al., 2017; Koop-Jakobsen and Gutbrod, 2019). Thus, considering the presence of ponds is necessary to accurately predict the landscape-level evolution and persistence of these salt marshes under climate change.

Ponds haven been simulated in a simplified 2D model (Kirwan et al., 2008) by lowering the elevation and preventing vegetation growth in a few random locations on the marsh platform. After this temporary disturbance, the vegetation was allowed to regrow and the bed quickly regained its original elevation by accreting faster than RSLR rate. Because of these localized and temporary bursts of vertical accretion, the model provided a simple explanation for the presence of spatial heterogeneities in marsh vertical accretion and for the widely observed mismatch between marsh vertical accretion and RSLR. Nonetheless, the model overlooked several physically-based processes that play a key role in pond dynamics: pond deepening by organic matter oxidation, pond expansion by erosion of the pond edge, and pond drainage by channel interception.

A simple lumped model that considered the evolution of a single pond (Mariotti, 2016) suggested that marshes are either in a regime of pond recovery where ponds form, expand, reconnect with the nearby tidal creek and recover to the surrounding marsh elevation, or in a regime of pond runaway (also called pond collapse regime) in which ponds do not revegetate and marsh area is lost even if the vegetated platform keeps pace with sea-level rise. Vertical accretion by *in situ* plant production does not contribute to pond recovery if, at the time of pond drainage, the elevation of the pond bed is below the limit for vegetation growth, which is roughly equal to mean sea level along the Atlantic and Gulf Coast of the USA (McKee

and Patrick, 1988). Indeed, if the bed elevation lies below the limit for vegetation growth, vertical accretion is only provided by deposition of suspended sediment. Vertical accretion by *in situ* plant production would be present only after the elevation deficit for vegetation growth is overcome. Accordingly, the model found that the marsh enters the pond runaway regime when the RSLR rate is larger than the minimum unvegetated accretion rate (Mariotti, 2016), which is equal to $C \cdot r/(2T \cdot \rho_m)$, where C is the suspended sediment concentration, r is the tidal range, T is the tidal period, and ρ_m is the mud dry bulk density. Marshes are thus more likely to be in the pond runaway regime if the tidal range is small, but a very large sediment supply can allow for pond recovery in microtidal systems, as shown by an example in coastal Louisiana (Mariotti, 2016). A major limitation of the model, however, was that it neglected the interactions between multiple ponds, which likely represent important spatial dynamics over long time scales. As a consequence, the model was not able to predict spatially averaged metrics, such as the amount of pond area on the marsh platform in the pond recovery regime or the rate of pond area increase in the pond runaway regime.

When considering the dynamics of ponds, it is also important to simulate key aspects of sediment transport. For example, it is crucial to simulate how the suspended sediment concentration (SSC) that drives inorganic deposition (i.e., mud) varies in space, such as the SSC decreases with distance from the channels (Christiansen et al., 2000; Fagherazzi et al., 2012), thus making the marsh interior more susceptible to entering the pond runaway regime. In addition, lateral sediment redistribution by soil diffusion (or soil creep), which is present along marsh boundaries with sharp elevation gradients such as the banks tidal creeks (Kirwan and Murray, 2007; Mariotti, 2018; Mariotti et al., 2016, 2019), could transfer sediment from high to low elevation areas and thus affect the rate of vertical elevation change.

Another important aspect to consider is the biogeochemical dynamics of ponds. The emergent vegetation that dominates the marsh platform (e.g., *Spartina alterniflora, S. patens, Distichlis spicata*, etc.) cannot survive in ponds because of inundation stress or because of the high salinity that results from the absence of regular flushing (Pethick, 1974). Instead, ponds in New England marshes are colonized by communities of micro- and macro-algae and submerged grasses such as *Ruppia maritima* (Harshberger, 1909; Spivak et

al., 2017). The organic matter composition of pond surface sediments reflects inputs from algal and plant communities that colonize ponds during formation (Spivak et al., 2018). Yet, the contribution of submerged algae and grasses to vertical accretion in ponds is likely negligible, given that ponds tend to be net heterotrophic (Spivak et al., 2017) and thus do not accumulate carbon but rather remove the existing marsh peat (Spivak et al., 2018).

In addition to the absence of vertical accretion, ponds might actually experience a net elevation loss. Indeed, the high rates of respiration, driven primarily by sulfate reduction (van Huissteden and van de Plassche 1998), convert buried organic matter into dissolved inorganic carbon and thereby contribute to soil column collapse and pond deepening (Johnston et al., 2003; Spivak et al., 2017, 2018). The elevation trajectory of ponds is thus diametrically opposite to that of the marsh platform, which gains elevation through time via suspended sediment deposition and *in situ* plant production. As a result, ponds in New England marshes are likely experiencing a gradual deepening with respect to the surrounding marsh platform (Wilson et al., 2009, 2010).

Here, we develop a spatially explicit model for pond dynamics. We apply the model to the Barnstable marsh (MA, USA), which is a typical mesotidal marsh in New England, and constrain the model with field data and remote sensing analysis. We also consider the case with a smaller tidal range, using as reference a nearby microtidal marsh with limited sediment supply (the Sage Lot Pond marsh). Then, we explore the model for different RSLR rates and sediment supply to predict future marsh trajectories. As suggested by a previous idealized model (Mariotti, 2016), we expect to find a threshold above which ponds never revegetate and thus lead to permanent marsh loss. By including pond dynamics within the model, we predict marsh loss when the marsh complex enters the runaway pond regime, which occurs even when deposition on the vegetated marsh platform is equal or greater than the RSLR rate, a commonly used threshold for marsh drowning (Morris et al., 2002).

2. Site description

115 The study area is in the New England region of the United States, which experiences a temperate climate,
116 about 1000 mm of precipitation per year, a growing season from May to September, and overnight freezes
117 during the winter (Mariotti et al., 2019). Ice rafting has been documented to occur, especially in
118 concomitance with winter storm surges (Argow et al., 2011).

119 Barnstable is a mesotidal backbarrier marsh, located on the north side of the Cape Cod peninsula (Fig. 1).
120 The spring tidal range is about 3.6 m (NOAA Sesuit Harbor station 8447241). The marsh is dominated by
121 *S. alterniflora* in the low marsh and *S. patens* in the high marsh (Redfield, 1972). The majority of the
122 Barnstable marsh has been ditched since the early 1900s. For simplicity, in this study we focus on an area
123 that does not have man-made ditches (Fig. 1). This choice allows us to isolate and understand the spatially
124 explicit pond dynamics under natural conditions, without the confounding effects of mechanical
125 anthropogenic disturbances.

126 Sage Lot Pond is a polyhaline, microtidal (0.7 m spring tidal range, NOAA Woods Hole Station 8447930)
127 backbarrier marsh located on the south side of the Cape Cod peninsula (Fig. 1). The marsh is dominated by
128 short form *S. alterniflora* on the low marsh and *Distichilis spicata, Juncus gerardii,* and some *S. patens* at
129 higher elevations (Gonneea et al. 2019). This marsh is also ditched.

130 According to the nearby NOAA station 8443970, mean sea level was -9.2 cm in the NAVD88 datum during
131 the epoch 1983-2001. Considering the recent increase in sea level, we assume that MSL is now at 0 m
132 NAVD88, which agrees with the datum analysis in the nearby Plum Island Estuary marsh (Hopkinson et
133 al., 2018).

134 ## 3. Methods

135 ### 3.1 Field measurements and remote sensing analysis

136 For the Barnstable marsh, suspended sediments in tidal creek water were collected in triplicate 1-liter pre-
137 combusted (450 ºC) glass bottles from four different locations (Fig. 1) between June 21st and August 1st
138 2018. Samples were filtered through pre-combusted and pre-weighed glass fiber filters (nominal pore size

139 0.45 μm). The filters were then dried to constant mass (60 ºC) and concentrations were calculated by
140 normalizing suspended sediment mass to the volume filtered. While this sampling is not a comprehensive
141 characterization of the sediment dynamics, it provides at least a magnitude estimate, which is often the only
142 data available (Cavatorta et al., 2003).

143 Sediment cores were collected from three transects at approximately 2 m (channel adjacent) and 100 m
144 (marsh interior) from the creek bank (Table 1). All cores were taken in the vegetated platform, i.e., not in a
145 pond. Cores were collected with a modified piston core where a plastic core liner (11 cm diameter) was
146 fitted with a gasketed piston and placed on the sediment surface. The core liner was pushed ~70 cm into
147 the marsh subsurface while the piston was maintained at the surface to minimize compaction, which was
148 observed through the clear core liner. The cores were split vertically, sampled at 1 cm intervals to 45 cm
149 below soil surface and 2 cm intervals thereafter, frozen, and then freeze-dried. Sediment samples were
150 prepared for gamma analysis by sealing approximately 5 g of dried, homogenized peat for 3 weeks, and
151 counting on a planar-type gamma counter for 24 to 48 hours to measure ^{7}Be, ^{137}Cs, ^{210}Pb, and ^{226}Ra at 477,
152 661.6, 46.5 and 352 KeV energies respectively (Canberra Inc., USA). Detector efficiency was determined
153 from EPA standard pitchblende ore in the same geometry as the samples. Activities of ^{7}Be, ^{137}Cs, and ^{210}Pb
154 were decay corrected to time of collection. Suppression of low energy peaks by self-adsorption was
155 corrected for according to (Cutshall et al., 1983). Excess ^{210}Pb was calculated by subtracting supported
156 ^{226}Ra from total ^{210}Pb with a detection limit of 0.1 dpm g^{-1}. Sediment ages were calculated using the
157 continuous rate of supply ^{210}Pb age model, a variant on the advection-decay equation (Appleby and
158 Oldfield, 1978). This age model assumes that ^{210}Pb down-core activity is a function of decay and variable
159 sediment accretion, however, the full ^{210}Pb profile must be captured to prevent bias towards ages that are
160 too old and accretion rates that are too low at depth (Binford, 1990). Vertical accretion rates were calculated
161 as the age difference between each interval, with temporal resolution typically 2 to 10 years depending on
162 marsh, treatment, and sediment age.

Ponds within a few hundred meters from the sites where cores were collected were surveyed in the summer of 2019 in one of two ways (Fig. 1G). First, 200 marsh-pond boundaries were surveyed in 2019 by measuring the elevation of the marsh adjacent to the pond edge and the elevation of the pond bed adjacent to the pond edge using an RTK-GPS with vertical accuracy of 2 cm. The height of the pond bank was calculated as the difference between these measurements. Second, elevation transects running through the diameter of the pond were surveyed for thirteen of the 200 ponds (five small, five medium, and three large ponds). The absolute bed elevation was referenced to the elevation of the adjacent marsh surface, which was surveyed with the RTK-GPS.

We performed a remote sensing analysis using two datasets: USGS Single Frames Aerial Photos from March 1973 with resolution of ~0.5 m and USGS high resolution orthoimages from April 2014 with resolution of 0.075 m, both of which were collected at low tide (earthexplorer.usgs.gov). We also used USGS Lidar collected in 2014 with resolution of 1 m (OCM Partners, 2019). For consistency we resampled all datasets to a 1 m resolution. In both images we defined isolated ponds as those cells with standing water at low tide, which were easily identifiable using a threshold on the intensity of the visible band. Pond cells were clustered together using a five-point stencil connection, such that pond cells that touched each other either on the top, bottom, right, or left boundary were grouped together. Then, we identified the same ponds in each image and calculated the rate of area change. We excluded from the analysis those ponds that either merged together or reconnected to the channel network between 1973 and 2014. From the rate of area change, we calculated the equivalent rate of pond radius expansion. Change was measured as a difference in area rather than the retreat of the pond edge, eliminating any error due to image misalignment.

For the Sage Lot Pond marsh, SSC was measured from 2011 to 2018 across all seasons and tides. A total of 258 grab samples (500 mL each) were collected and stored at 4 ºC for a maximum of 1 week and then filtered through pre-combusted borosilicate glass fiber filters (0.7 um pore size), rinsed thoroughly with deionized water to remove salts, and dried at 105 ºC for >4h. SSC was determined as the ratio of dried

187 filtrate mass total per sample volume. Existing vertical accretion measurements for Sage Lot Pond marsh
188 (Gonneea et al., 2019, 2018) are also reported in Table 1.

189 **3.2 Model for pond dynamics**

190 Within the model, the pond dynamics is implemented as a cellular automata, in which each cell is described
191 by its state (which can only take a finite number of values) without explicitly simulating the elevation.
192 Channels are special cells that are fixed in time, which do not widen, narrow, or migrate laterally. These
193 cells don't take part in the evolution of the cellular automata and are collectively defined as "channel
194 network". Cells that are not part of the channel network are marsh cells, which collectively constitute the
195 marsh domain. Marsh cells are either connected or isolated. Connected cells experience tidal fluctuations,
196 and are defined as vegetated platform if their elevation is above the lower limit for vegetation growth (z_{min})
197 or mudflat if their elevation is below (z_{min}). Isolated cells, also called isolated ponds or ponds, do not
198 experience tidal fluctuations or exchange with the channel network. Pond cells with an elevation below z_{min}
199 are defined as drowned ponds (Fig. 2).

200 Two processes allow for connected marsh cells to become isolated cells: pond formation and pond
201 expansion. In the real marsh, formation of new ponds can take place by a variety of mechanisms. A slight
202 depression in the marsh might lead to increased water logging and rapid decay of the marsh peat (Spivak et
203 al., 2018). Deposition of rafts composed of either eroded plant material or macroalgae might kill the
204 standing vegetation and temporarily prevent new plant growth (Pethick, 1974). Ice rafting might compress
205 the marsh (Argow and FitzGerald, 2006) or remove large pieces of standing vegetation. Sub-surface piping
206 might collapse the marsh from below (Kesel and Smith, 1978). Large patches of vegetation can be removed
207 by grazers such a geese herbivory (Kirwan et al., 2008) and major storms (Howes et al., 2010). Rather than
208 explicitly modeling these different mechanisms, we simply assume that individual ponds form at a constant
209 rate k_{seed} [#ponds/m^2/yr], that is, during each time step Δt, each vegetated marsh cell is transformed into a
210 pond cell with a probability $k_{seed}\Delta t\Delta x^2$. Pond expansion allows existing ponds (i.e., clusters of connected
211 pond cells) to enlarge. This process is implemented at every boundary between a pond cell and a vegetated

cell. Expansion is simulated using a probabilistic approach (Mariotti and Canestrelli, 2017), in which a vegetated cell adjacent to a pond cell is converted to a pond cell with a probability $p=k_{exp}\Delta t/\Delta x$, where k_{exp} is the expansion rate [m/yr].

Pond cells transform into vegetated cells though pond drainage. In the real marsh, pond drainage occurs when a pond becomes close enough to the channel network that a new connecting channel forms, as exemplified in Fig. 1E. Then, the pond fills in quickly (assuming that there is enough sediment supply) and the connecting channel, now lacking the tidal prism associated with the pond, eventually silts in. The model is unable to explicitly simulate the formation or closure of these transient connecting channels, since the model does not simulate tidal hydrodynamics and the main channel network is assumed to be fixed in time. We thus parameterize this effect by assuming that pond drainage instantaneously occurs when a connected cell becomes closer than a critical distance L from the channel network. When this happens, the whole pond, which consists of all pond cells that are contiguous to at least one pond cell with distance L from the channel network, are drained and all its cells become connected cells. The distance L is the distance at which the pressure gradient generated by the water in the pond is able to start scouring the marsh soil – possibly by seepage and piping first – and eventually form a connecting channel. In theory, this distance might be calculated using a hydrodynamic and sediment transport model, but for simplicity this distance is calibrated to reproduce the observation that ponds tend to drain when they get about 20 m away from the main channel network (Fig. 1E).

3.3 Model for elevation dynamics

The elevation of each marsh cell relative to mean sea level, $z(x,y,t)$, is described as

$$\frac{\mathrm{d}z}{\mathrm{d}t} = D_p + D_m - S - P - R \quad \text{(Eq. 1)}$$

where D_p is the *in situ* organic accretion by marsh plants, D_m is the accretion from suspended sediment, which we assume is composed of mud and thus transported in suspension, S is the divergence of the creep

flux F, P is the elevation loss by pond dynamics (which is further explained below), and R is the relative sea-level rise rate.

The organic accretion by *in situ* plant production is $D_p=D_{pMAX}B$, where D_{pMAX} is the maximum accretion rate [mm/yr] and B is a function that describes the dependence on the bed elevation and serves as a proxy for the hydroperiod, $B = \max[0, 4(z - z_{min})(z_{max} - z)/(z_{max} - z_{min})^2\ ]$, where z_{min} and z_{max} are the minimum and maximum elevation for vegetation growth. B is set equal to zero in isolated ponds, simulating the absence of marsh plants and assuming that any macrophytes and microphytobenthos present in ponds do not contribute to substantial vertical accretion.

Mud accretion depends on hydroperiod and the local SSC. The spatial pattern of SSC is described by

$$C = C_o\left(\alpha + (1-\alpha)e^{-\beta l}\right) \quad \text{(Eq. 2)}$$

where C_o is the time-average suspended sediment concentration in the channels, $l(x,y)$ is the distance to the closest cells that belong to the channel network, β is the decay factor for SSC with distance from the channel network, and α is the factor describing the SSC that is spatially uniform. This last parameter allows transport of sediment even to large distances from the channels, and thus can parameterize processes such as storm-induced deposition on the marsh platform. Mud accretion thus equals

$$D_m = \frac{C\min(h, r)\min(1, h/\Delta r)}{T\rho_m} \quad \text{(Eq. 3)}$$

where h is the depth with respect to MHHW, T is the tidal period, ρ_m is the dry bulk density of the mud, and Δr is the difference between the spring and neap high tide. The last factor in the numerator is introduced to account for modulation introduced by the spring-neap variability. If the marsh elevation is at least Δr lower than MHHW, the marsh is inundated every tidal cycle and this factor is equal to one. If the marsh is higher than this elevation, the marsh is only inundated during spring tides, and the factor will be less than one. This allows mud to deposit at high marsh elevations but at a lower rate.

In theory, ponds could accrete vertically by suspended sediment deposition akin to the marsh platform. Yet, several reasons suggest that this deposition is small. First, despite ponds having a large depth, the water in the pond is not exchanged during tides. Only the thin layer of water that flows over the pond should count toward sediment deposition as formulated in Eq. 3 (which assumes that the water depth is equal to the depth of the flow that floods that cell). Second, ponds lack the emergent marsh vegetation that enhances sediment trapping. As a consequence, for the same water depth and sediment concentration, a vegetated pond should experience a lower sediment deposition that a vegetated marsh. Third, ponds are generally far from channels, specifically they are always farther than the distance L. As such, the suspended sediment concentration above ponds is always lower than on the marsh close to the channel edge. Furthermore, field data suggested that ponds in a New England salt marsh are isolated from the tidal network and do not import sediment (Spivak et al., 2017). Overall, sediment deposition in the ponds is likely very small, and for simplicity is set equal to zero.

The creep flux F parameterizes all processes that cause soil diffusion and is set equal to $\mu\nabla z$, where μ is the soil diffusivity coefficient, whose value was empirically found equal to ~0.1 m^2/yr (Mariotti et al., 2019). The creep flux is set equal to zero within ponds and, more importantly, at the pond edges. This choice reflects the absence of tidal oscillations, a process that creates "tidal fatigue" and is responsible for the fast creep in channel banks (Mariotti et al., 2019). This is due to the standing water in the isolated ponds maintaining hydrostatic pressure on the pond bank and preventing slumping during low tide. Thus, the model allows isolated ponds to have relatively steep banks, as observed in the field (Wilson et al., 2010). When pond cells reconnect, they drain instantaneously, and creep can take place. Excluding the creep process at the edge of isolated ponds results in isolated pond expansion only occurring according to the pond expansion term k_{exp}, which can be calibrated by direct comparison with the observed historical expansion rate of isolated ponds. To summarize, creep does not affect isolated pond dynamics, but does affect the dynamics of mudflats (i.e., connected ponds) and prevents the formation of an unrealistically

large elevation gradient in the marsh interior, which in reality might have been smoothed by hydrodynamic processes other than creep but that the model is unable to explicitly simulate.

The channel dynamics is not explicitly simulated, and the channel elevation is kept equal to the lower limit for vegetation growth. This elevation acts as a boundary condition for the bed elevation gradients and thus affects the sediment creep flux near the banks. Noticeably, creep from the marsh platform into the channels moves material out of the marsh domain and thus acts as a sink. Creep can also redistribute sediment within the marsh domain; this does not count as either a sink or source because it conserves sediment.

Finally, the term P includes the platform elevation loss through pond processes. When a connected cell becomes a pond cell by either pond formation or pond expansion, it loses the elevation $Y=\min(Y_{max}, \max(0, z-z_{min}))$, where Y_{max} is the maximum scour thickness, calibrated with field data, and z_{min} is the lower elevation limit below which pond scour does not occur. Y is the thickness of the material that is instantaneously removed from the system, such that the elevation z is lowered by the amount Y.

The term P also includes pond deepening, which simulates organic matter decomposition via sulfate reduction in the bed of the pond. Pond deepening is set equal to a constant rate ($P_{deepening}$) if $z>z_{min}$ and to zero if $z<z_{min}$. Even though we introduced active pond deepening to simulate the loss of elevation caused by organic matter decomposition, this term could be more generally considered as the net effect of all the processes that change pond elevation. For example, if we assume that some sediment settles in the pond during high tide, the term $P_{deepening}$ should be interpreted as the net deepening, including the actual pond deepening by organic matter decomposition minus the elevation gain caused by sediment deposition. If sediment deposition was larger than organic matter decomposition, $P_{deepening}$ could be negative, and the pond might gain elevation through time. Given that this parameter is calibrated by comparing measured and modeled pond depths, not by directly measuring the deepening or accretion, we are unable to isolate these two components.

To summarize, the pond depth, relative to the surrounding marsh platform, is controlled by three mechanisms: 1) the initial scour, which takes place by either pond formation or expansion, 2) the active

306 pond deepening, and 3) the relative deepening caused by the surrounding marsh gaining elevation through
307 organic and inorganic accretion.

308 **3.4 Coupling between pond dynamics and elevation dynamics**

309 As outlined above, the bed elevation is affected by pond processes of formation, expansion, and deepening
310 through the term P (Eq. 1). While the cellular automata model formulated in Section 2.2 is independent of
311 bed elevation, the elevation dynamics is introduced by allowing ponds to form and expand only in vegetated
312 marsh cells. This rule keeps ponds from forming and expanding into a mudflat, which is defined as a
313 connected cell with an elevation lower than z_{min}. This model implementation is a result of only allowing the
314 processes associated with isolated pond formation and expansion to occur in highly organic soil that can be
315 oxidized and compressed.

316 If the pond elevation at the time of drainage is higher than z_{min}, the pond revegetates just after it is drained.
317 In other words, the cell instantaneously switches from a pond to a vegetated marsh status. In this scenario,
318 every cell that is not a pond is a vegetated marsh that can be transformed back to a pond through either
319 pond formation or pond expansion. In this case, the pond dynamics without elevation is equivalent to the
320 pond dynamics with elevation, so the cellular automata can be run independently of the elevation. On the
321 other hand, if the connected ponds do not revegetate immediately, they become mudflat cells in which
322 ponds are not allowed to form (because $z<z_{min}$). These areas affect the dynamics of pond formation and
323 expansion, and thus the cellular automata model needs to be run together with the elevation model.

324 A special consideration should be given to cells whose elevation drops below the vegetation limit z_{min}.
325 These cells can be either drowned ponds or mudflats (Fig. 2). Neither has organic accretion by vegetation
326 (Eq. 3), but only the mudflat cells receive inorganic sediment and are allowed to creep under the model
327 specifications. If a drowned pond is surrounded by mudflats, the pond cannot expand. As a result, drowned
328 ponds will never intercept a channel and will never drain in the model domain. In reality, drowned ponds
329 should connect to the channel network through channels that quickly form in the mudflats, but these are not
330 explicitly simulated in the model. Connecting these drowned ponds to creeks will not immediately allow

for pond revegetation since the pond is still below the vegetation limit, but it will allow for inorganic accretion and creep, which will both increase the bed elevation and potentially allow for revegetation. In the model we account for this dynamic by introducing the rule that any drowned pond that touches a mudflat becomes a mudflat itself, and receives inorganic sediment. Then, the evolution of the mudflat would follow the elevation dynamics as previously described.

To summarize, the pond dynamics can be affected by the presence of mudflat cells, since ponds cannot form or expand into these cells. The formation of mudflats is controlled by active pond deepening ($P_{deepening}$) and by RSLR; the recovery of mudflats is controlled by mud accumulation and by RSLR (Fig. 2). If the amount of mudflats at any time is negligible (a few percent of the total marsh area), then the elevation dynamics would in practice not affect the pond dynamics.

4. Results

4.1 Field measurements

The pond expansion rate, calculated using remote sensing, was equal to ~1.5 cm/yr, with a weak dependence on the pond size (Fig. 3). This is calculated for ponds that did not merge between 1973 and 2014 and thus only includes ponds smaller than about 20 m. We were not able to measure expansion for larger ponds. Detailed transects across thirteen ponds indicate that ponds are 0.3-1.2 m deep and that their depth increases with diameter. The survey of 200 marsh-pond boundaries revealed that the depth of the pond immediately adjacent to the bank was 0.46±0.21 m. As such, the depth of the pond close to the edge is relatively uniform, whereas the depth in the middle of the pond has a greater variability. Field measurements at Barnstable marsh show an accretion of 4.6±2.5 mm/yr near the channel and 5.1±3.3 mm/yr in the marsh interior over the past 100 years (Table 1). Total suspended sediment concentrations were 29.3±3.6 mg/l for Barnstable and 5.0±2.8 mg/l for Sage Lot pond.

4.2 Pond dynamics not coupled to elevation

354 The model simulations were run in a portion of the Barnstable marsh about 1.2 x 1.2 km (Fig. 1C). Using
355 the 2014 Lidar topography, the channel network was defined as the area with an elevation lower than the
356 limit for vegetation growth, which was assumed to be equal to MSL. Areas that were identified as ponds
357 (Section 2.1) were excluded from the channel network.

358 The pond model is first run without including the requirement that ponds can only form and expand where
359 the marsh elevation is greater than z_{min}. In this case, the pond dynamics does not depend on bed elevation.
360 This simplification is equivalent to the fully coupled model if the pond elevation never drops below z_{min},
361 and it is nearly equivalent to the fully coupled model if the amount of mudflats is negligible, which is the
362 case if mudflats recover quickly. The advantage of running the model without the elevation dynamics is to
363 emphasize a key feature of pond dynamics, that is, the spatial distribution of ponds does not depend on
364 RSLR and sediment supply. As such, the parameters for pond evolution (k_{seed} and k_{exp}) can be calibrated
365 against observations without being affected by the uncertainties associated with RSLR (and its variability
366 during the last century) and sediment supply (which is estimated using a limited number of samples).

367 Starting with a marsh without ponds, we run the model for 1000 years to reach a steady state, defined as
368 the period in which the time-averaged statistical distribution of ponds does not change. We found that pond
369 dynamics does not depend on the size of the ponds formed via the seeding mechanism, rather the same
370 steady state pond distribution is obtained if the ponds formed by the seeding mechanism are composed of
371 a single or several cells (and thus the initial ponds is larger). This occurs because the amount of pond area
372 created by seeding, where ponds are introduced into the model, is small compared to the area gained by
373 pond expansion. As such, the main effect of pond formation is not to directly increase the pond area, but
374 rather to create "seeds" that allow for pond expansion. This also confirms that pond formation should have
375 units of #ponds$\cdot m^{-2}yr^{-1}$ and not of $m^2m^{-2}yr^{-1}$.

376 We found that the steady state pond size distribution only depends on the ratio between pond formation and
377 expansion rates. This is confirmed by noticing that the ratio between the two rates has units of #ponds/m^3
378 and is independent of time. The actual values of the rates only affect the time needed to reach the steady

state distribution. The ratio between pond formation and expansion rate that best fits the pond size distribution (Fig. 4) is 0.027 #ponds/m^3. If the ratio decreases, the number of small ponds decreases while allowing for only a few large ponds (Fig. 4). Intuitively, in this scenario each pond has more time to expand before eventually being drained. Using the measured pond expansion rate (1.5 cm/yr), the pond formation rate is estimated to be $4 \cdot 10^{-4}$ ponds$\cdot m^{-2} yr^{-1}$. We could not directly measure this rate because of the difficulty of detecting small ponds.

4.3 Elevation dynamics

Simulations that include the elevation dynamics (Section 2.3) are run for 1000 years, in which the first 900 years have R of 1 mm/yr and the last 100 years have R of 2.9 mm/yr, thus representing the RSLR acceleration in the 19th century (NOAA Woods Hole Station 8447930). Thus, year 900 of the simulation roughly corresponds to year 1914, whereas year 1000 roughly corresponds to year 2014 (i.e., present time). The model at year 0 is initialized with an elevation equal to the 90th percentile of the vegetation range, i.e., $0.9(r/2)$=1.62 m. Despite this initialization of marsh elevation being arbitrary, it does not affect the results after about 500 years. Put differently, any initial marsh elevation would lead to the (statistically) same results during the last few hundred years of the simulation. As such, this approach recreates a synthetic marsh representative for the beginning of the 20th century that is 1) at steady state according to the processes included in the model, 2) independent of any arbitrary initial marsh elevation, 3) independent of any topography measured at present time. Specifically, the measured Lidar is not used to initialize the marsh elevation nor the pond distribution. Only the geospatial distribution of channels (which could be reconstructed from aerial images without elevation) is needed to initialize the model.

First, we consider the elevation dynamics without the presence of ponds (Fig. 5). We analyze this scenario by considering the spatially averaged vertical fluxes over the marsh domain (Fig. 6). As expected, the net vertical accretion is equal to the RSLR rate. When RSLR rate increases to 2.9 mm/yr, the net vertical accretion lags behind, but it nearly matches the RSLR rate after about 100 years (i.e., at present times). The gross vertical accretion at present times is 5.1 mm/yr. This value represents the spatially averaged accretion

rate; in reality the accretion is much higher in the marsh adjacent (<10 m) to channels, where it can be up to 20 mm/yr (Figs. 5, 7C). This additional accretion is balanced by bank creep, which transports sediment out of the marsh domain. When spatially averaged over the entire marsh, this creep flux creates an equivalent deficit of 2.2 mm/yr, which allows the net vertical accretion to balance the RSLR rate (Fig. 6).

Next, we run the model including the mechanisms of pond formation, expansion, and deepening. The maximum initial pond depth Y_{max} (which is both the maximum initial scour of new ponds, as well as the maximum initial scour when the pond edge expands) is set equal to the measured height of the pond edge, which was measured for Barnstable marsh to be 0.46 m. The consequences of this choice in the model are that 1) small ponds would have a nearly uniform depth across the pond, and that depth would be about 0.46 m, 2) larger ponds would have a depth greater than 0.46 m in their center, which is older and thus may have deepened over time due to organic matter decomposition as well as accretion of the adjacent marsh platform, whereas their edges, which formed recently, would have a depth of ~0.46 m. The active pond deepening $P_{deepening}$ was instead calibrated to match the observed depth in the middle of the ponds (Fig. 8). As expected, the pond depth is much greater in the middle than at the edge, and the depth in the middle of the pond increases with the pond diameter.

Ponds do not affect the marsh dynamics in the buffer zone close to the channel network, where ponds are drained instantaneously. This is equivalent to assuming that they do not form at all and cannot expand. As such, the model that includes pond dynamics has a similar pattern of bank creep and excess accretion on the marsh adjacent to the channel as the model without pond dynamics (Fig. 6). On the other hand, ponds drastically change the dynamics of the marsh interior. Ponding creates a heterogeneous landscape, with low elevation areas surrounded by high marsh areas. This elevation pattern is mirrored by a spatially heterogeneous vertical accretion, where the net vertical accretion in ponds is zero (if not negative, because of active pond deepening), whereas recently connected ponds experience enhanced vertical accretion. Compared to the case without ponds, the average marsh elevation is also lower.

Because pond reconnection is a stochastic process, the vertical accretion rate is not constant in time. In particular, there are periods when large ponds are drained and the vertical accretion suddenly increases (Fig. 6). Over a sufficient time period (e.g. 50 years), however, the net vertical accretion rate is equal to R.

4.4 Exploring the effects of RSLR rate, sediment supply, and tidal range

To generalize our results, we perform a series of explorative simulations with different sediment supplies (C_o), RSLR rates (R), and tidal ranges (r). In order to consistently initialize the simulations, we start with a uniform elevation equal to $0.9(r/2)$ with no ponds, and then run the model with R equal to 1 mm/yr for 500 years, which is enough to establish a steady state pond distribution (Fig. 6). As already pointed out, the choice of the initial elevation does not affect the results after about 500 years. After 500 years, we changed a single parameter (either R or C_o) while keeping all the other parameters fixed, and run the simulations for an additional 1000 years (Fig. 9). We focused on scenarios in which the vegetated marsh kept pace with RSLR and thus all marsh loss is due to pond expansion.

First, we consider the effects on increasing R or decreasing C_o in a mesotidal marsh such as Barnstable marsh. For the relatively high sediment supply of Barnstable marsh (C_o=30 mg/l), the RSLR rate does not affect the dynamics of ponds, which always occupies ~10% of the marsh. For the case with a lower C_o=10 mg/l, lower R gives nearly identical results as for the case with a higher C_o, with pond area remaining at ~10% of the total marsh area, whereas high R starts to affect pond area (Fig. 9A). For example, for C_o=10 mg/l and R=8 mm/yr, the total unvegetated area (ponds plus mudflats) increases to about 25% within 500 years (Fig. 9A). Noticeably, under these conditions, the unvegetated area stabilizes and does not increase indefinitely even after 1000 years.

Next, we consider the case of a marsh with a smaller tidal range. We use as a reference Sage Lot Pond marsh, which has a spring tidal range of 0.7 m (Gonneea et al. 2019). Field measurements indicate that this marsh has a small sediment supply equal to 5 mg/l. For simplicity, we consider the same channel geometry as of Barnstable marsh but with a smaller tidal range. Accordingly, we modify the vegetation limit, the initial marsh elevation, the maximum initial pond elevation, and the spring-neap variability (Table 2). For

453 the microtidal case, we found that for low *R* the unvegetated area is still ~10%, but for higher rates the
454 unvegetated area increases quickly, and can be up to 100%, indicating loss of the entire the marsh platform
455 (Fig. 9B). The model predicts that the marsh would enter the pond runaway regime for *R*~3 mm/yr (Fig.
456 9B).

457 We also compared the model predictions with the measured accretion rates in Barnstable and Sage Lot
458 Pond marsh. We separated the spatially averaged accretion predicted by the model between the marsh
459 adjacent to channels (less than 10 m from the nearest channel, which roughly coincides with the low marsh,
460 and is about 29% of the total marsh area) and the marsh interior (more than 10 m from the nearest channel,
461 where bank creep is virtually zero, and is about 71% of the total marsh area). For a marsh with low tidal
462 amplitude and sediment supply such as Sage Lot Pond, the model predicts that when RSLR rate was 1
463 mm/yr , the gross vertical accretion rates was ~2.6 mm/yr in the marsh adjacent to channels and ~1.4 mm/yr
464 for the marsh interior (Fig. 7B). After the acceleration in RSLR to 2.9 mm/yr the model predicts that the
465 gross vertical accretion increases to ~4.1 mm/yr in the marsh adjacent to the channels and to ~3 mm/yr in
466 the marsh interior (Fig. 7B). For comparison, the field measurements of accretion over a 100 year period,
467 which includes the period during modern RSLR acceleration, indicate an accretion rate of 3.7±2.0 mm/yr
468 close to the channels and 1.4±0.3 mm/yr in the interior (Table 1). For the Barnstable marsh, with a higher
469 tidal range and sediment supply, the model predicts gross vertical accretion rates of ~9.5 mm/yr near
470 channels and ~2.8 mm/year in the marsh interior when RSLR rate is 1 mm/yr, and ~11.5 mm/yr near
471 channels and ~4.0 mm/year in the marsh interior when RSLR rate is 2.9 mm/yr (Fig. 7A). For comparison,
472 field measurements at Barnstable marsh show an accretion of 4.6±2.5 mm/yr near the channel and 5.1±3.3
473 mm/yr in the marsh interior over the past 100 years.

474 As an indicator of the overall marsh status, we calculated the spatially-averaged primary productivity
475 normalized by the maximum productivity (Fig. 9). The productivity of the vegetated marsh depends on the
476 bed elevation following the function *B* (section 3.3), whereas the productivity in the ponds is equal to zero.
477 As the RSLR rate increases, the marsh elevation decreases and thus the productivity increases. As the

478 unvegetated pond area starts to increases, however, the overall marsh productivity starts to decrease. This
479 is particularly evident for the Sage Lot Pond marsh for a RSLR rate greater than 4 mm/yr (Fig. 9B).

480 Finally, we expanded these simulations by systematically considering different tidal ranges (0.7, 1.6, 3.6
481 m), RSLR rates (1 to 8 mm/yr), and sediment supply concentrations (5 to 30 mg/l) (Fig. 10). We found that,
482 for small tidal ranges, the rate of marsh loss by pond expansion is highly sensitive to the RSLR rate. When
483 the RSLR rate increases to 3 mm/yr, marsh loss occurs but is relatively slow, and the amount of unvegetated
484 area (which includes both ponds and mudflats) increases from 10% to 15% of the total marsh area during
485 the first 100 years (Fig. 9). A further increase in the RSLR rate (5 mm/yr) drastically increases the rate of
486 marsh loss, with the amount of unvegetated area increasing from 10% to 40% of the total marsh area during
487 the first 100 years.

488 **5. Discussion**

489 **5.1 The pervasive effect of ponds in salt marshes**

490 Ponds in Barnstable marsh expand at a very slow rate (1.5 cm/yr) compared to exposed marsh creekbank
491 edges that retreat by wave-induced erosion (0.5-10 m/yr) (Marani et al., 2011; Leonardi et al., 2016;
492 Hopkinson et al., 2018; Elsey-Quirk et al., 2019). Yet, ponds are numerous and collectively have a long
493 perimeter, and thus are able to affect nearly the entire marsh surface on millennial time scales. Considering
494 an average unchanneled length of 50 m (Marani et al., 2003), a pond formed in the middle of the marsh
495 would take ~2000 years to reach an area influenced by channel network and drain. Since some ponds form
496 closer to the channel network initially, 2000 years is likely an upper estimate of the time needed to reconnect
497 ponds to the channel network and drain. In addition, ponds that merge together will drastically reduce the
498 time needed for a pond to reconnect to the channel network.

499 Given that the Barnstable marsh is ~4000 years old (Redfield, 1965), we expect that any point on the marsh
500 was at least once a pond. Indeed, stratigraphic evidence of ponds were found in nearly all cores taken in a
501 New England salt marsh (ME, USA) (Wilson et al., 2009). However, many historical records within salt

marshes only extend ~100 years, due to age model constraints of the commonly used lead-210 methods, and thus may miss some of these millennial scale dynamics. In any case, the assumption of steady state marsh accretion often used while interpreting the sedimentary record (Morris et al., 2016) should be evaluated, since even if RLSR rate and sediment supply are constant, a specific site within the marsh may not be at steady state at any given time due to pond dynamics.

Another consequence of pond dynamics is that recently connected ponds (as identified in Fig. 1E) are a common feature and should be interpreted as part of the basic marsh dynamics as opposed to an indicator of changes in boundary conditions. Thus, ponds do not necessarily indicate an acceleration in RSLR or other anthropogenic modifications, but are rather a natural occurrence within many salt marshes. Ponds also create diverse habitats and ecological niches for wildlife (Brush et al., 1986), and thus should not necessarily be considered a negative feature within salt marshes.

5.2 Vertical accretion in the pond recovery regime

When the marsh is in the pond recovery regime, pond dynamics in the marsh interior increased the spatially-averaged gross vertical accretion by 0.5-2 mm/yr (Fig. 7), a result that was previously predicted (Kirwan et al., 2008). This excess accretion is larger for larger tidal ranges, because marshes with a larger tidal range have a thicker soil profile that can be removed by the ponding processes. Ponding also results in highly heterogeneous accretion across the marsh platform (Fig. 5), and thus the excess accretion rate during pond recovery could locally be much higher than 2 mm/yr. For example, the model predicts that recovering ponds might have accretion rates up to 20 mm/yr (Fig. 5). Indeed, Wilson et al., (2014) reported vertical accretion rates of 8 mm/yr in recently recovered ponds in a New England salt marsh, despite the fact that the sediment supply in that marsh was extremely low (~5 mg/l). The model predicts that the excess accretion rate persists from when a pond revegetates until it reaches the equilibrium elevation with the marsh surface. In other words, ponds that were drained centuries ago might not have fully equilibrated and thus might still accrete slightly faster than the RSLR rate. These predictions are consistent with the 5.1 mm/yr vertical accretion

526 measured in the marsh interior of Barnstable marsh during a period when relative sea-level rise rate was
527 2.9 mm/y (NOAA Woods Hole Station 8447930) (Table 1).

528 Our model also predicts channel bank creep causes an equivalent elevation drop of ~2 mm/yr when
529 averaged over the whole marsh platform (Fig. 6,7). This loss is balanced by an excess vertical accretion
530 (Mariotti et al., 2016), which can be observed by the gross vertical accretion rate being much larger than
531 the RSLR rate. Contrary to ponding, this bank creep is localized to the low marsh immediately adjacent to
532 channels, where the excess vertical accretion can be an order of magnitude higher than RSLR rate (i.e., up
533 to 20 mm/yr, Fig. 5). This prediction is consistent with the larger vertical accretion rates measured on the
534 marsh adjacent to channels than on the marsh interior at Sage Lot Pond marsh (Table 1). For Barnstable
535 marsh, the model predicts that the vertical accretion on the marsh adjacent to channels is ~11 mm/yr (Fig.
536 7A), which is much larger than the measured 4.6±2.5 mm/yr (Table 1). One possible explanation is that the
537 channel-adjacent area in the model integrates portions of the marsh that are extremely low (e.g., the
538 vegetated bank located a few meters from the channel). These low areas have a disproportionally high
539 excess accretion (Fig. 5 and Fig. 7C,D) and strongly influence the average value over the area here defined
540 as channel-adjacent (<10 m from the channel network). Field measurements in the channel-adjacent area,
541 in contrast, are generally taken a few meters inland from the edge of the marsh, with a higher elevation than
542 the slumping blocks and where the excess accretion is much lower. Indeed, the cores in Barnstable collected
543 ~2 m from the marsh edge are actually ~5 m from the lowest vegetated point (Fig. 1H). Noticeably, the
544 model predicts a minimum in vertical accretion, equal to about 3 mm/yr, located between 5 and 20 m from
545 the channel (Fig. 7C). This is the region where neither bank creep nor ponding are present, and thus the
546 gross accretion rate matches RSLR rate.

547 The model also recreates the lagged vertical accretion that follows the acceleration in RSLR rate, a
548 disequilibrium effect has been previously identified with simplified marsh models (Kirwan and Murray,
549 2008; Kirwan and Temmerman, 2009). This lag should be present in every salt marsh that experienced
550 accelerated RSLR, regardless of pond occurrence or the influence of bank creep.

To summarize, the model is able to combine three previously identified mechanisms by which vertical accretion rates deviate from the RSLR rate, emphasizing that a direct comparison between vertical accretion and RSLR rate can be misleading at best, and overly optimistic for projecting marsh elevation trajectories.

5.3 Vertical accretion in the pond runaway regime

The simple lumped model (Mariotti, 2016) identified the minimum unvegetated accretion, $D_{cr}=C\cdot r/(2T\cdot\rho_m)$, as the threshold between pond recovery and pond runaway regimes. Because C is not spatially uniform, D_{cr} varies among the domain. D_{cr} is lowest in the marsh interior, where $D_{cr}=\alpha\cdot C_o\cdot r/(2T\cdot\rho_m)$.

For $R<D_{cr}$, the lumped pond model predicts that every pond recovers. Indeed, the spatially explicit model predicts that, for any RSLR rate lower than D_{cr}, ponds always occupy ~10% of the marsh area (Figs. 9,10). This prediction agrees with the finding that stable salt marshes are associated with an unvegetated-vegetated ratio of ~0.1 (Wasson et al., 2019) (a pond area of 10% corresponds to an unvegetated-vegetated ratio of 0.11). As for the lumped model, the spatially explicit model predicts an increase in the total unvegetated area as $R>D_{cr}$. The spatially explicit model provides more information than the lumped model, and specifically predicts that the rate at which marsh loss by pond expansion takes place strongly increases as R further exceeds D_{cr}. Put differently, when R is just slightly above D_{cr}, the rate of marsh loss by pond expansion is extremely low, and the marsh could last thousands of years. On the other hand, once the threshold for pond runaway is exceeded, even small increases in R could have catastrophic consequences for marsh loss.

Using D_{cr} as the threshold for the pond runaway regime is further complicated by the presence of creep, which can take place at the edge of mudflats (i.e., connected ponds). Creep transfers sediment from high to low elevations, and thus tends to increase vertical accretion in the mudflats and to lower vertical accretion on the vegetated platform. For example, a very small mudflat might recover even if R is slightly larger than D_{cr} (which explains why the Sage Lot Pond marsh does not enter the pond runaway regime for R=1 mm/yr even if D_{cr}=0.6 mm/yr). Lateral transport of sediment not associated with creep, including sediment transport by waves or sheet flow over the marsh, might slightly alter the predictions purely based on vertical

accretion rates. Nonetheless, the parameter D_{cr} captures the transition to the pond runaway regime within an uncertainty of about 1 mm/yr (Fig. 10).

5.4 Pond formation

A crucial parameter in the model is the rate of pond formation. If ponds do not form, neither the pond recovery nor the pond runaway regime occurs. In this case, the marsh is either fully vegetated or disappears by drowning, and thus the marsh landscape is dramatically different than what simulated in our model (Fig. 5). As such, it is noteworthy to emphasize that ponds are not always present in salt marshes. Ponds have been identified in the Mid-Atlantic and New England Coast of the USA (Adamowicz and Roman, 2005; Mariotti, 2016; Schepers et al., 2017) as well as in the northern Gulf of Mexico (Nyman et al., 1994; Mariotti, 2016). Yet, marshes in the South-Atlantic Coast of the USA, including sites with relatively little human modifications such as in Virginia and Georgia, seem to have few ponds if any at all. For marshes in which ponds are not common, it is possible that either ponds do not form at all or that the pond formation rate (the parameter k_{seed}) is extremely low. In this latter case the model would predict that the number of ponds would be highly reduced (Fig. 4) and that their size distribution would be highly skewed towards a few large ponds.

In this study, we assumed that ponds form without explicitly simulating the mechanisms that lead to pond formation in the first place. In particular, we did not investigate whether the rate of pond formation changes as a function of environmental drivers. We can only speculate that pond formation might be related to disturbances related to climate via ice rafting and scour, excessive wrack accumulation, grazing/bioturbation such as by *Sesarma reticulatum* crab or burrowing species such as fiddler crabs (*Uca* sp.), and to biogeochemical and hydrological processes associated with microtopography.

We further emphasize that pond formation *per se* is not directly driving permanent marsh loss, but it could lead to marsh loss in the pond runaway regime. In the pond runaway regime, an increase in the pond formation rate would directly increase the rate at which the marsh is lost, mainly by increasing the "seeds" from which ponds can expand. Pond formation is thus an example of a relatively secondary mechanism

601 that, through spatial interactions (Larsen, 2019), could lead to rapid marsh loss. Thus, we argue that future
602 research should develop a mechanistic understanding of pond formation and determine whether
603 environmental changes such climate or burrowing and grazing pressure, might increase the rate of pond
604 formation.

605 **5.5 Marsh management**

606 All simulations were performed for scenarios in which the vegetated marsh keeps pace with RSLR. As
607 such, if pond dynamics were not included, the marsh would have been preserved indefinitely and there
608 would have not been any unvegetated area occupied by either ponds or mudflats. Thus, including pond
609 dynamics in marshes where ponds are known to form is an essential step to simulate marsh evolution.

610 Including pond dynamics in marsh models is also essential for predicting ecosystem productivity. Marsh
611 grasses remove CO_2 from the atmosphere and bury it in soils, support coastal food webs, and filter inorganic
612 nutrients washed from the landscape, among other ecosystem services. As such, changes in productivity
613 have consequences for ecological and biogeochemical processes within marshes and adjacent ecosystems.
614 In both the mesotidal (Barnstable) and microtidal (Sage Lot Pond) simulations, normalized primary
615 productivity increases monotonically with the RSLR rate (Fig. 9). The expansion of the unvegetated area
616 for very high RSLR rates, however, starts to decrease productivity. For the microtidal case, a decrease in
617 productivity associated with pond expansion could be observed even at the decadal time scale (Fig. 9B),
618 and thus could be relevant for coastal management.

619 As previously identified (Mariotti, 2016), neither the presence of ponds nor the expansion of ponds is a sign
620 of permanent marsh loss. On the other hand, the absence of pond recovery is a potential indicator of a
621 regime shift. Monitoring pond recovery, such as by measuring their accretion rates once reconnected to the
622 channel network, should thus become a routine marsh assessment, alongside measurements of vertical
623 accretion in the vegetated marsh.

One management question is whether to promote or prevent pond recovery. One example includes selectively digging ditches to reconnect ponds, a strategy referred to as "quality ditching" or Open Water Marsh Management (Wolfe, 1996). Our model suggests that the appropriate management (in terms of morphological evolution of the salt marsh) depends on whether the marsh is in the pond recovery or pond runaway regime. In the former case, favoring pond drainage should accelerate vertical accretion, in the latter it would accelerate marsh loss.

As previously shown in a model that only considers one pond (Mariotti, 2016), determining whether a marsh is in the pond runaway or pond recovery regimes requires an estimate of the minimum inorganic deposition in the marsh interior (D_{cr}), and specifically to estimate the suspended sediment concentration. Because this parameter is difficult to determine without long-term monitoring (Ganju et al., 2017), we suggest that analyzing the trajectory of recently connected ponds is important to determine whether ponds are recovering or expanding indefinitely.

5.6 Model limitations and future directions

The model assumes that any connected area above z_{min} revegetates instantaneously. Therefore, a mudflat is only present if $z<z_{min}$. In reality it could take several years for a connected pond to revegetate even if $z>z_{min}$. For example, the recently connected ponds in Barnstable have not fully revegetated even if their elevation is ~1 m above MSL (i.e., $z>z_{min}$). Even though this delay could be included in the dynamics, we argue that it is not crucial, because revegetation likely will occur within shorter times scales (decades) than the time scale considered in this study. More importantly, large vertical accretion rates by mud deposition could take place even though recently connected ponds are not fully revegetated.

Channels are assumed to be fixed. When analyzing historical imagery (~50 years), channels in Barnstable marsh are relatively stable, even though they could have migrated over longer time scales. Migrating channels would likely increase the rate at which ponds are intercepted and thus drained. Channel migration could be parameterized as a larger value for the reference drainage distance L, allowing ponds within the model to drain even if located at a large distance from channels. Indeed, this could be a dominant

mechanism for pond drainage at sites where channel migration is relatively fast (Finotello et al., 2018). Channel migration would likely result in similar marsh evolution dynamics and pond recovery, with marsh loss at the eroding bank but, at the same time, induce accretion that is faster than the RSRL rate at the accreting bank.

The model does not conserve sediment in the channel domain: the sediment transported from the bank to the channel through the creep mechanism does not accumulate in the channel, and the sediment transported from the channel to the marsh, which is responsible for the term D_m, does not cause a sediment deficit in the channel network. That is, we assume that there is an infinite supply of new sediment from the channels. In reality, a portion of the bank material that creeps into the channel would be resuspended and re-transported to the marsh platform, thus allowing for sediment recycling. This component cannot be reproduced in the model, since an explicit representation of the channel dynamics would be needed.

Finally, the model does not include the dynamics of hydrological alterations such as ditching, which is a common feature in New England salt marshes. Ditching could impact the marsh elevation dynamics in at least two ways. On one hand, ditches could cause a nearly instantaneous marsh-wide pond drainage, which could temporarily increase the spatially averaged vertical accretion rate. On the other hand, ditches could lower the water table and cause a combination of carbon oxidation and compaction, which in turn could lower the marsh elevation. Such effects could be included in the model by 1) allowing ponds close to the ditches to be drained similarly to the ponds drained by the natural channel network, and 2) adding an additional term in Eq. 1 to simulate a localized bed lowering close to the ditches.

6. Conclusions

The proposed model simulates the spatially explicit dynamics of marsh ponds, and thus allows simulation of the aggregated effect that ponds have on the evolution of the marsh platform. The Barnstable marsh is predicted to be in a pond recovery regime: pond expansion does not cause net marsh loss because they recover the marsh elevation once drained. Even in the pond recovery regime, however, ponds drastically affect the marsh elevation and vertical accretion. In particular, pond dynamics explain why marsh vertical

674 accretion, even away from channels, could be several times larger than the rate of RSLR, and also why the
675 accretion rate is highly variable in space.

676 The model predicts that future increases in RSLR rate at Barnstable marsh would not cause the marsh to
677 transition to the full pond runaway regime. Yet, with a large RSLR rate and a reduced sediment supply,
678 ponds in the marsh interior might become permanent mudflats and thus increase the unvegetated area to
679 ~20% of the total marsh. Monitoring of pond recovery, such as by measuring their accretion rates once
680 reconnected to the channel network, could be used as a landscape-level indicator of regime shifts.

681 Marshes with a smaller tidal range and sediment supply, such as Sage Lot Pond marsh, are more prone to
682 enter the pond runaway regime. For RSLR rates just above the critical threshold (e.g., 3 mm/yr), the rate of
683 marsh loss by pond expansion is still relatively low, and the marsh could take several centuries (if not
684 millennia) before completely disappearing. A further acceleration in RSLR rate (e.g., 5 mm/yr) would
685 drastically increase the rate at which the marsh is lost by pond expansion – which will take place even
686 though the vegetated marsh keeps pace with RSLR.

687 Future research needs include understanding the mechanism of pond formation, evaluating how
688 hydrological alterations such as ditching affects pond dynamics, and quantifying how pond dynamics affect
689 blue carbon accumulation and preservation.

690

691 **Acknowledgments**

692 We appreciate funding support for this work from Woods Hole Sea Grant (NA14OAR4170104 to ACS and
693 GM) and NOAA NSC (NA14NOS4190145 to ACS, GM, MEG, and MT), USGS Coastal & Marine
694 Geology Program, the USGS Land Change Science Program's LandCarbon program. We thank the
695 Waquoit Bay National Estuarine Research Reserve and Sandy Neck Beach Park for providing research
696 access. USGS staff including T. Wallace Brooks, Jennifer O'Keefe Suttles, Adrian Mann and Allyson
697 Boggess provided field and analytical support. Additional field support was provided by Claire Mayorga,

Kelsey Gosselin, Madelyn Francesconi, and Sam MicNichol. Any use of trade, firm or product names is for descriptive purposes only and does not imply endorsement by the U.S. Government.

References

Adamowicz, S.C., Roman, C.T., 2005. New England salt marsh pools: A quantitative analysis of geomorphic and geographic features. Wetlands 25, 279–288. https://doi.org/10.1672/4

Appleby, P.G., Oldfield, F., 1978. The calculation of lead-210 dates assuming a constant rate of supply of unsupported 210Pb to the sediment. Catena 5, 1–8. https://doi.org/10.1016/S0341-8162(78)80002-2

Argow, B.A., FitzGerald, D.M., 2006. Winter processes on northern salt marshes: Evaluating the impact of in-situ peat compaction due to ice loading, Wells, ME. Estuar. Coast. Shelf Sci., Salt Marsh Geomorphology: Physical and ecological effects on landform 69, 360–369. https://doi.org/10.1016/j.ecss.2006.05.006

Argow, B.A., Hughes, Z.J., FitzGerald, D.M., 2011. Ice raft formation, sediment load, and theoretical potential for ice-rafted sediment influx on northern coastal wetlands. Cont. Shelf Res. 31, 1294–1305. https://doi.org/10.1016/j.csr.2011.05.004

Binford, M.W., 1990. Calculation and uncertainty analysis of 210Pb dates for PIRLA project lake sediment cores. J. Paleolimnol. 3, 253–267. https://doi.org/10.1007/BF00219461

Brush, T., Lent, R.A., Hruby, T., Harrington, B.A., Marshall, R.M., Montgomery, W.G., 1986. Habitat Use by Salt Marsh Birds and Response to Open Marsh Water Management. Colon. Waterbirds 9, 189–195. https://doi.org/10.2307/1521212

Cavatorta, J.R., Johnston, M., Hopkinson, C., Valentine, V., 2003. Patterns of sedimentation in a salt marsh-dominated estuary. Biol. Bull. 205, 239–241.

720 Christiansen, T., Wiberg, P.L., Milligan, T.G., 2000. Flow and Sediment Transport on a Tidal Salt Marsh
721 Surface. Estuar. Coast. Shelf Sci. 50, 315–331. https://doi.org/10.1006/ecss.2000.0548

722 Cutshall, N.H., Larsen, I.L., Olsen, C.R., 1983. Direct analysis of 210Pb in sediment samples: Self-
723 absorption corrections. Nucl. Instrum. Methods Phys. Res. 206, 309–312. https://doi.org/10.1016/0167-
724 5087(83)91273-5

725 Elsey-Quirk, T., Mariotti, G., Valentine, K., Raper, K., 2019. Retreating marsh shoreline creates hotspots
726 of high-marsh plant diversity. Sci. Rep. 9, 5795. https://doi.org/10.1038/s41598-019-42119-8

727 Fagherazzi, S., Kirwan, M.L., Mudd, S.M., Guntenspergen, G.R., Temmerman, S., D'Alpaos, A., Koppel,
728 J., Rybczyk, J.M., Reyes, E., Craft, C., others, 2012. Numerical models of salt marsh evolution: Ecological,
729 geomorphic, and climatic factors. Rev. Geophys. 50.

730 Finotello, A., Lanzoni, S., Ghinassi, M., Marani, M., Rinaldo, A., D'Alpaos, A., 2018. Field migration rates
731 of tidal meanders recapitulate fluvial morphodynamics. Proc. Natl. Acad. Sci. 115, 1463–1468.
732 https://doi.org/10.1073/pnas.1711330115

733 Ganju, N.K., Defne, Z., Kirwan, M.L., Fagherazzi, S., D'Alpaos, A., Carniello, L., 2017. Spatially
734 integrative metrics reveal hidden vulnerability of microtidal salt marshes. Nat. Commun. 8.
735 https://doi.org/10.1038/ncomms14156

736 Gonneea, M.E., Maio, C.V., Kroeger, K.D., Hawkes, A.D., Mora, J., Sullivan, R., Madsen, S., Buzard,
737 R.M., Cahill, N., Donnelly, J.P., 2019. Salt marsh ecosystem restructuring enhances elevation resilience
738 and carbon storage during accelerating relative sea-level rise. Estuar. Coast. Shelf Sci. 217, 56–68.
739 https://doi.org/10.1016/j.ecss.2018.11.003

740 Gonneea, M.E., O'Keefe Suttles, J.A., Kroeger, K.D., 2018. Collection, analysis, and age-dating of
741 sediment cores from salt marshes on the south shore of Cape Cod, Massachusetts, from 2013 through 2014.
742 US Geol. Surv. Data Release Httpsdoiorg105066F7H41QPP.

743 Harshberger, J.W., 1909. The Vegetation of the Salt Marshes and of the Salt and Fresh Water Ponds of
744 Northern Coastal New Jersey. Proc. Acad. Nat. Sci. Phila. 61, 373–400.

745 Hopkinson, C.S., Morris, J.T., Fagherazzi, S., Wollheim, W.M., Raymond, P.A., 2018. Lateral Marsh Edge
746 Erosion as a Source of Sediments for Vertical Marsh Accretion. J. Geophys. Res. Biogeosciences 123,
747 2444–2465. https://doi.org/10.1029/2017JG004358

748 Howes, N.C., FitzGerald, D.M., Hughes, Z.J., Georgiou, I.Y., Kulp, M.A., Miner, M.D., Smith, J.M.,
749 Barras, J.A., 2010. Hurricane-induced failure of low salinity wetlands. Proc. Natl. Acad. Sci. 107, 14014–
750 14019. https://doi.org/10.1073/pnas.0914582107

751 Johnston, M.E., Cavatorta, J.R., Hopkinson, C.S., Valentine, V., 2003. Importance of metabolism in the
752 development of salt marsh ponds. Biol. Bull. 205, 248–249.

753 Kesel, R.H., Smith, J.S., 1978. Tidal creek and pan formation in intertidal salt marshes, Nigg Bay, Scotland.
754 Scott. Geogr. Mag. 94, 159–168. https://doi.org/10.1080/00369227808736403

755 Kirwan, M., Temmerman, S., 2009. Coastal marsh response to historical and future sea-level acceleration.
756 Quat. Sci. Rev., Quaternary Ice Sheet-Ocean Interactions and Landscape Responses 28, 1801–1808.
757 https://doi.org/10.1016/j.quascirev.2009.02.022

758 Kirwan, M.L., Murray, A.B., 2008. Tidal marshes as disequilibrium landscapes? Lags between morphology
759 and Holocene sea level change. Geophys. Res. Lett. 35, L24401. https://doi.org/10.1029/2008GL036050

760 Kirwan, M.L., Murray, A.B., 2007. A coupled geomorphic and ecological model of tidal marsh evolution.
761 Proc. Natl. Acad. Sci. 104, 6118–6122. https://doi.org/10.1073/pnas.0700958104

762 Kirwan, M.L., Murray, A.B., Boyd, W.S., 2008. Temporary vegetation disturbance as an explanation for
763 permanent loss of tidal wetlands. Geophys. Res. Lett. 35, n/a–n/a. https://doi.org/10.1029/2007GL032681

764 Koop-Jakobsen, K., Gutbrod, M.S., 2019. Shallow Salt Marsh Tidal Ponds–An Environment With Extreme
765 Oxygen Dynamics. Front. Environ. Sci. 7. https://doi.org/10.3389/fenvs.2019.00137

766 Larsen, L.G., 2019. Multiscale flow-vegetation-sediment feedbacks in low-gradient landscapes.
767 Geomorphology 334, 165–193. https://doi.org/10.1016/j.geomorph.2019.03.009

768 Leonardi, N., Ganju, N.K., Fagherazzi, S., 2016. A linear relationship between wave power and erosion
769 determines salt-marsh resilience to violent storms and hurricanes. Proc. Natl. Acad. Sci. 113, 64–68.

770 Marani, M., Belluco, E., D'Alpaos, A., Defina, A., Lanzoni, S., Rinaldo, A., 2003. On the drainage density
771 of tidal networks. Water Resour. Res. 39, 1040. https://doi.org/10.1029/2001WR001051

772 Marani, M., D'Alpaos, A., Lanzoni, S., Santalucia, M., 2011. Understanding and predicting wave erosion
773 of marsh edges. Geophys. Res. Lett. 38, L21401. https://doi.org/10.1029/2011GL048995

774 Marani, M., Lio, C.D., D'Alpaos, A., 2013. Vegetation engineers marsh morphology through multiple
775 competing stable states. Proc. Natl. Acad. Sci. 201218327. https://doi.org/10.1073/pnas.1218327110

776 Mariotti, G., 2018. Marsh channel morphological response to sea level rise and sediment supply. Estuar.
777 Coast. Shelf Sci. https://doi.org/10.1016/j.ecss.2018.05.016

778 Mariotti, G., 2016. Revisiting salt marsh resilience to sea level rise: Are ponds responsible for permanent
779 land loss? J. Geophys. Res. Earth Surf. 121, 1391–1407. https://doi.org/10.1002/2016JF003900

780 Mariotti, G., Canestrelli, A., 2017. Long-term morphodynamics of muddy backbarrier basins: Fill in or
781 empty out? Water Resour. Res. 53, 7029–7054. https://doi.org/10.1002/2017WR020461

782 Mariotti, G., Kearney, W., Fagherazzi, S., 2016. Soil creep in salt marshes. Geology 44, 459–462.

783 Mariotti, G., Kearney, W.S., Fagherazzi, S., 2019. Soil creep in a mesotidal salt marsh channel bank: Fast,
784 seasonal, and water table mediated. Geomorphology 334, 126–137.
785 https://doi.org/10.1016/j.geomorph.2019.03.001

786 McKee, K.L., Patrick, W.H., Jr., 1988. The relationship of smooth cordgrass (Spartina Alterniflora) to tidal
787 datums: A review. Estuaries 11, 143–151. https://doi.org/10.2307/1351966

788 Morris, J.T., Barber, D.C., Callaway, J.C., Chambers, R., Hagen, S.C., Hopkinson, C.S., Johnson, B.J.,
789 Megonigal, P., Neubauer, S.C., Troxler, T., Wigand, C., 2016. Contributions of organic and inorganic
790 matter to sediment volume and accretion in tidal wetlands at steady state. Earths Future 4, 110–121.
791 https://doi.org/10.1002/2015EF000334

792 Morris, J.T., Sundareshwar, P.V., Nietch, C.T., Kjerfve, B., Cahoon, D.R., 2002. Responses of coastal
793 wetlands to rising sea level. Ecology 83, 2869–2877. https://doi.org/10.2307/3072022

794 Nyman, J.A., Carloss, M., Delaune, R.D., Patrick, W.H., 1994. Erosion rather than plant dieback as the
795 mechanism of marsh loss in an estuarine marsh. Earth Surf. Process. Landf. 19, 69–84.
796 https://doi.org/10.1002/esp.3290190106

797 OCM Partners, 2019. 2013-2014 U.S. Geological Survey CMGP LiDAR: Post Sandy (MA, NH,
798 RI), https://inport.nmfs.noaa.gov/inport/item/49846.

799 Pethick, J.S., 1974. The distribution of salt pans on tidal salt marshes. J. Biogeogr. 1, 57–62.
800 https://doi.org/10.2307/3038068

801 Redfield, A.C., 1972. Development of a New England Salt Marsh. Ecol. Monogr. 42, 201–237.
802 https://doi.org/10.2307/1942263

803 Redfield, A.C., 1965. Ontogeny of a Salt Marsh Estuary. Science 147, 50–55.
804 https://doi.org/10.1126/science.147.3653.50

805 Schepers, L., Kirwan, M., Guntenspergen, G., Temmerman, S., 2017. Spatio-temporal development of
806 vegetation die-off in a submerging coastal marsh. Limnol. Oceanogr. 62, 137–150.
807 https://doi.org/10.1002/lno.10381

808 Spivak, A.C., Gosselin, K., Howard, E., Mariotti, G., Forbrich, I., Stanley, R., Sylva, S.P., 2017. Shallow
809 ponds are heterogeneous habitats within a temperate salt marsh ecosystem. J. Geophys. Res. Biogeosciences
810 122, 1371–1384. https://doi.org/10.1002/2017JG003780

811 Spivak, A.C., Gosselin, K.M., Sylva, S.P., 2018. Shallow ponds are biogeochemically distinct habitats in
812 salt marsh ecosystems. Limnol. Oceanogr. 63, 1622–1642. https://doi.org/10.1002/lno.10797

813 van Huissteden, J., van de Plassche, O., 1998. Sulphate reduction as a geomorphological agent in tidal
814 marshes ('Great Marshes' at Barnstable, Cape Cod, USA). Earth Surf. Process. Landf. 23, 223–236.
815 https://doi.org/10.1002/(SICI)1096-9837(199803)23:3<223::AID-ESP843>3.0.CO;2-I

816 Wasson, K., Ganju, N.K., Defne, Z., Endris, C., Elsey-Quirk, T., Thorne, K.M., Freeman, C.M.,
817 Guntenspergen, G., Nowacki, D.J., Raposa, K.B., 2019. Understanding tidal marsh trajectories: evaluation
818 of multiple indicators of marsh persistence. Environ. Res. Lett. 14, 124073. https://doi.org/10.1088/1748-
819 9326/ab5a94

820 Wilson, C.A., Hughes, Z.J., FitzGerald, D.M., Hopkinson, C., Valentine, V., Kolker, A.S., 2014. Saltmarsh
821 Pool and Tidal Creek Morphodynamics: Dynamic Equilibrium of Northern Latitude Saltmarshes?
822 Geomorphology. https://doi.org/10.1016/j.geomorph.2014.01.002

823 Wilson, K.R., Kelley, J.T., Croitoru, A., Dionne, M., Belknap, D.F., Steneck, R., 2009. Stratigraphic and
824 Ecophysical Characterizations of Salt Pools: Dynamic Landforms of the Webhannet Salt Marsh, Wells,
825 ME, USA. Estuaries Coasts 32, 855–870. https://doi.org/10.1007/s12237-009-9203-7

826 Wilson, K.R., Kelley, J.T., Tanner, B.R., Belknap, D.F., 2010. Probing the origins and stratigraphic
827 signature of salt pools from north-temperate marshes in Maine, U.S.A. J. Coast. Res. 1007–1026.
828 https://doi.org/10.2112/JCOASTRES-D-10-00007.1

829 Wolfe, R.J., 1996. Effects of open marsh water management on selected tidal marsh resources: a review. J.
830 Am. Mosq. Control Assoc. 12, 701–712.

831

832 **List of figures**

Figure 1. A) Map of the study area including Barnstable marsh and Sage Lot Pond marsh (Massachusetts, USA). B) Sage Lot Pond marsh, C) Barnstable marsh. The dashed rectangle outlines the domain used in the model. The white dots indicate the locations where SSC was measured in triplicates. The red dots indicated the location were cores for vertical accretion were collected. D,E,F) Example of pond reconnection and rapid revegetation (the pond is indicated by the arrow on the bottom right of panel C). G) Location of the surveyed ponds. Red dots indicate ponds surveyed along a transect (showed in Fig. 8), white dots indicate ponds only surveyed at one edge. H) Detail of a marsh core collected adjacent to the channel. Images from Google Earth (NASA, USDA) accessed on October 2019.

Figure 2. Summary schematic of the marsh and pond dynamics and scheme of the various sediment fluxes in the model. Net vertical accretion is equal to the gross vertical deposition minus bank creep and ponding.

Figure 3. Measured pond edge expansion rate as the increase of the pond radius through time in Barnstable marsh from 1973 to 2014 as a function of the pond diameter.

Figure 4. A,B,C) Comparison of measured and modeled (at steady state after 1000 years) pond size distribution. A) Measured pond size distribution, showing that the total fraction of pond area is about 10% of the marsh surface. B) Best fit for the parameters k_{seed} and $k_{exp.}$. C) Model results for the case in which k_{seed} is decreased by a factor 100. D,G) Measured pond spatial distribution and elevation E,F,H,I) Model snapshot after 1000 years showing the pond spatial distribution and the elevation (as the last datapoint in Fig. 6).

Figure 5. Vertical accretion rate by *in situ* plant production and by mud accumulation for the case with and without pond dynamics calculated at year 1000 (as the last datapoint in Fig. 6). The inset in the top left panels shows the detail of the low-marsh adjacent to a channel.

Figure 6. Reconstructed time series of spatially-averaged elevation change for Barnstable marsh, comparing the case without ponds dynamics (A) and with pond dynamics (B). Gross accretion is the sum of plant and

856 mud accretion. Net accretion is the gross accretion minus ponding and bank creep. Note that during the first
857 ~500 years the marsh is equilibrating from the initial conditions without ponds.

858 Figure 7. A,B) Spatially-averaged elevation change during the transition from R=1 mm/yr to R=2.9 mm/yr
859 (as in Fig. 6B), considering the whole marsh area, the area adjacent to channels, and the marsh interior.
860 Note that in the marsh interior the bank creep is zero. C,D) Snapshot at year 1000 showing the how the
861 vertical accretion varies rapidly with the distance from the channel network. A,C) Conditions representing
862 Barnstable marsh (r=3.6 m, C_o=30 mg/l), B,D) Conditions representing Sage Lot Pond marsh (r=0.7 m,
863 C_o=5 mg/l).

864 Figure 8. A,B) Modeled 10th percentile (A) and mean (B) pond elevation as a function of pond size. The
865 blue dots are the individual points from the model, the red dots are the survey of the 13 ponds in Barnstable
866 marsh. C) Cross sections of the 13 ponds surveyed in Barnstable marsh (see Fig 1G).

867 Figure 9. A,B) Amount of pond and mudflat area through time for different RSLR rates for the case of
868 Barnstable marsh (r=3.6 m) with a reduced sediment supply (C_o=10 mg/l) (A), and for the case of Sage Lot
869 Pond marsh (r=0.7 m and C_o=5 mg/l) (B). The normalized primary production is calculated averaging the
870 plant primary production divided by the maximum primary production (which is attained when the marsh
871 is at the elevation optimum). The normalized primary production initially increases because the marsh
872 attains a lower elevation but subsequently decreases when the pond area (whose primary production is
873 assumed to be zero) increases. C) Snapshots of marsh configurations at different times (as indicated by the
874 black dots in panel B) for the case of Sage Lot Pond marsh with R=4 mm/yr.

875 Figure 10. Predictions of total unvegetated area (ponds + mudflats) at different time intervals after the
876 increase in RSLR rate. The dashed lines indicate the threshold between pond recovery and pond runaway
877 regime using the lumped pond model of Mariotti (2018), with $R=D_{cr}=\alpha C_o r/(2T\rho_m)$. The comparison with
878 Barnstable and Sage Lot Pond marsh is made assuming that the increase in relative sea level rise rate started
879 about 100 years ago at the beginning of the 20th century.

880 Table 1. Sediment accretion rates measured on 1 cm sediment core intervals in Barnstable (measured for
881 this work) and Sage Lot Pond marshes (Gonneea et al., 2019, 2018).

882 Table 2. List of parameters used in the model.

883

884

885

886

887

888

889

890

891

892

893

894

895

896

897

898

899

900

901

902 Figure 1

903

904 Figure 2

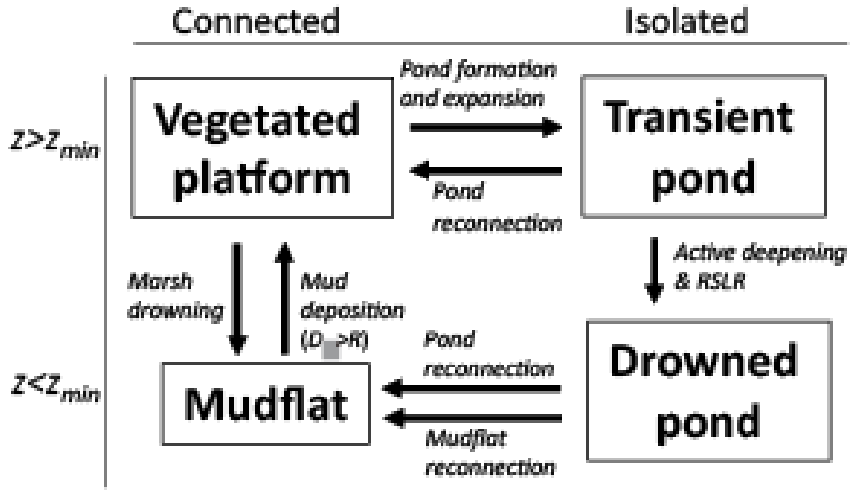

905

906

907 Figure 3

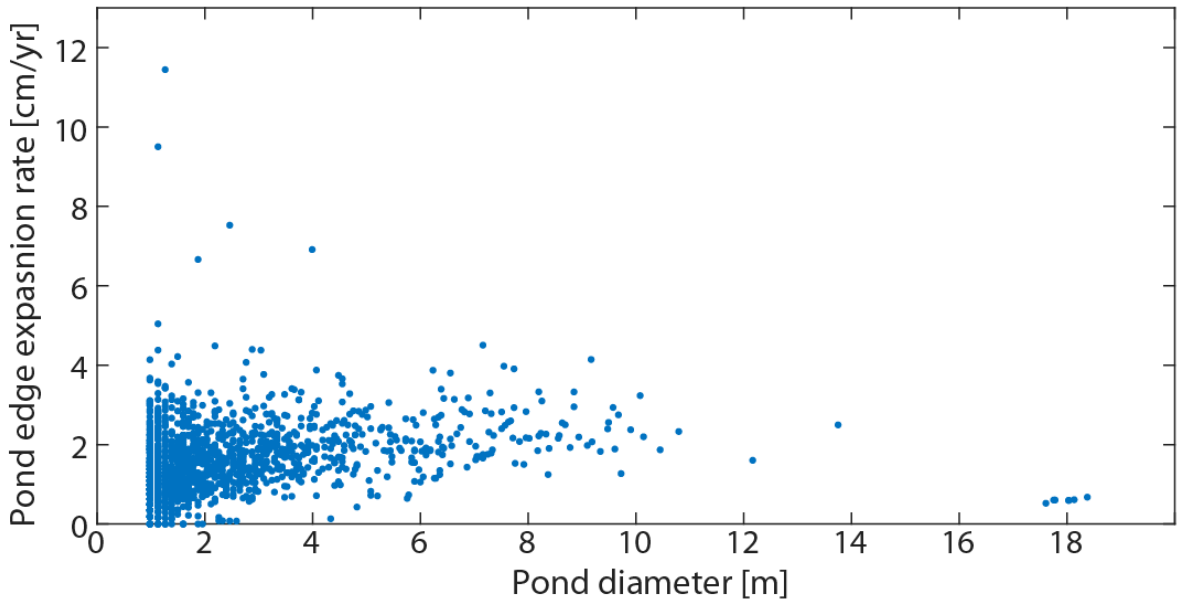

908

909

910 Figure 4

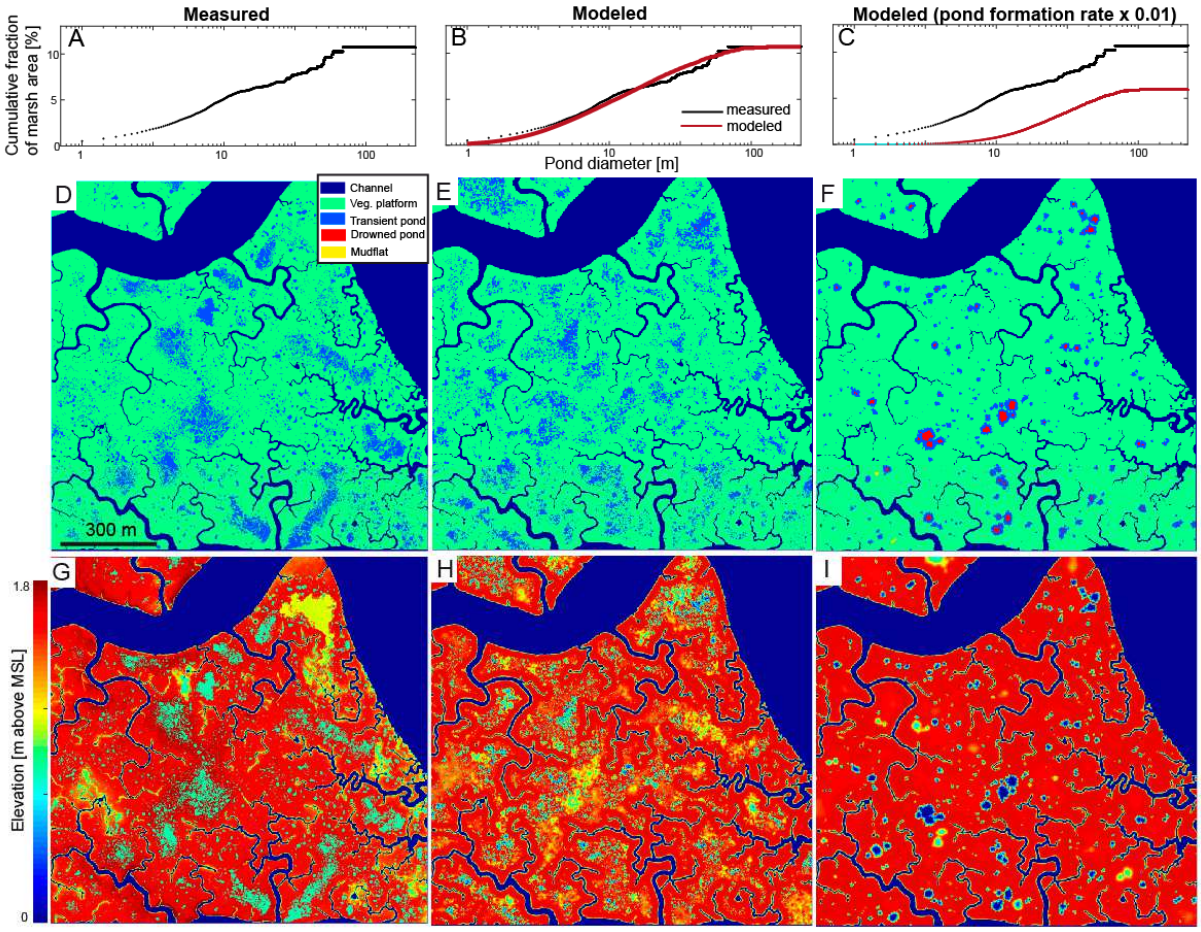

911

912

913 Figure 5

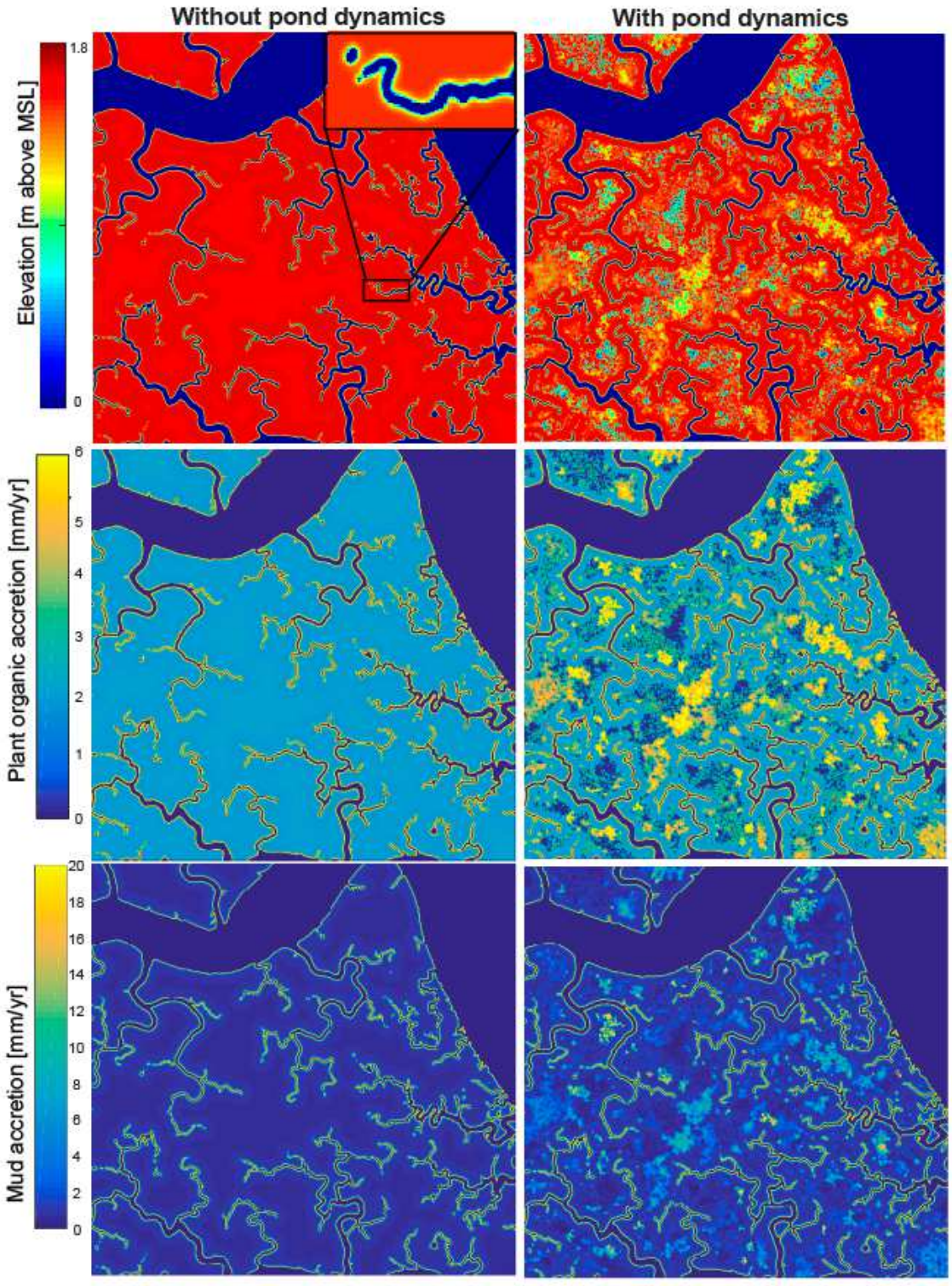

914

915

916 Figure 6

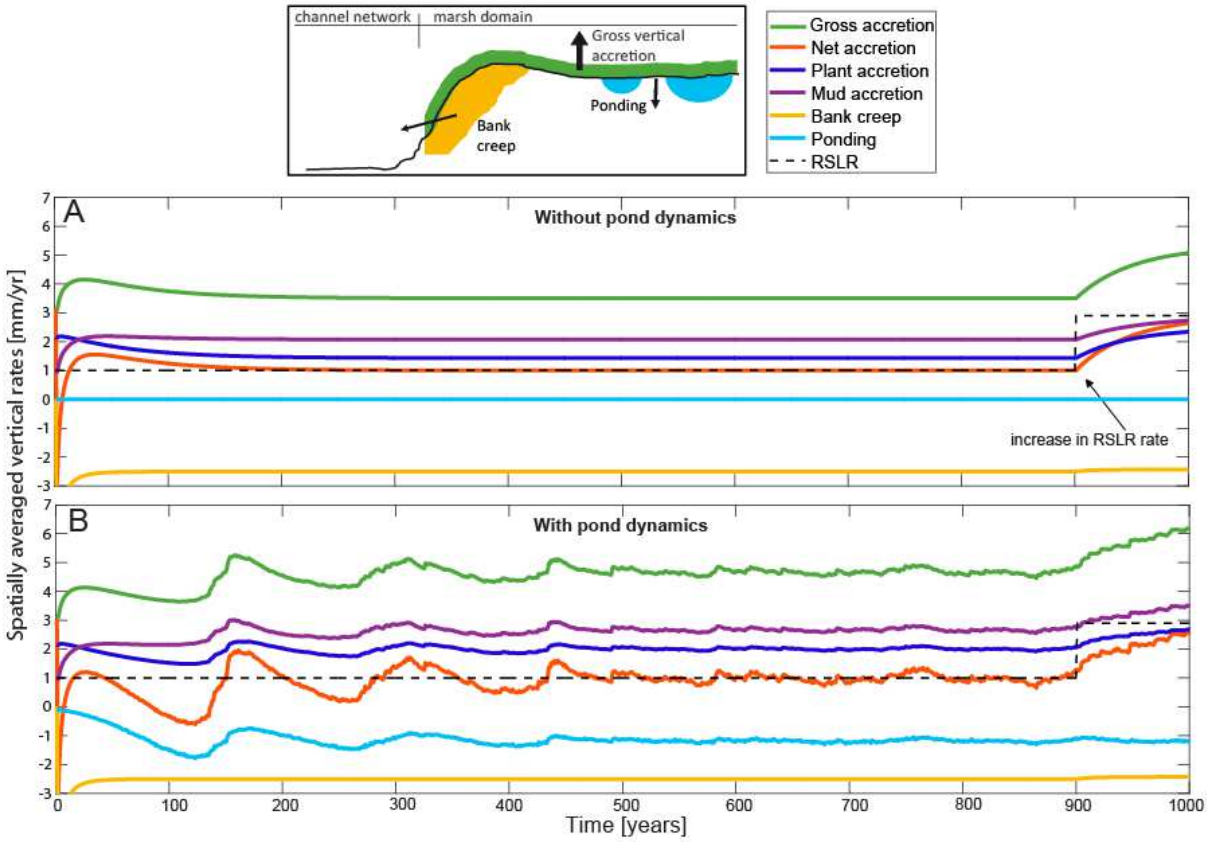

917

918

919 Figure 7

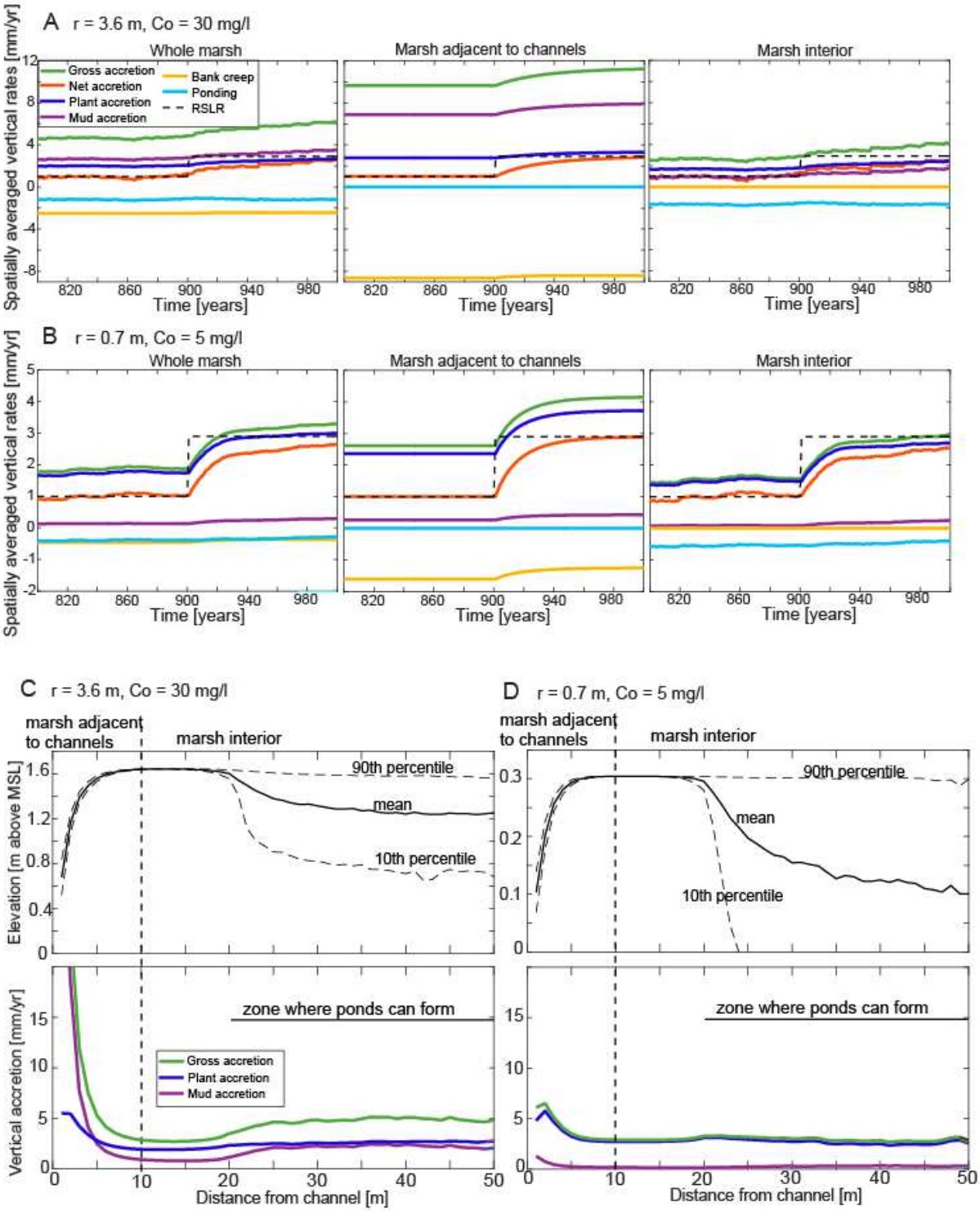

920

921

922 Figure 8

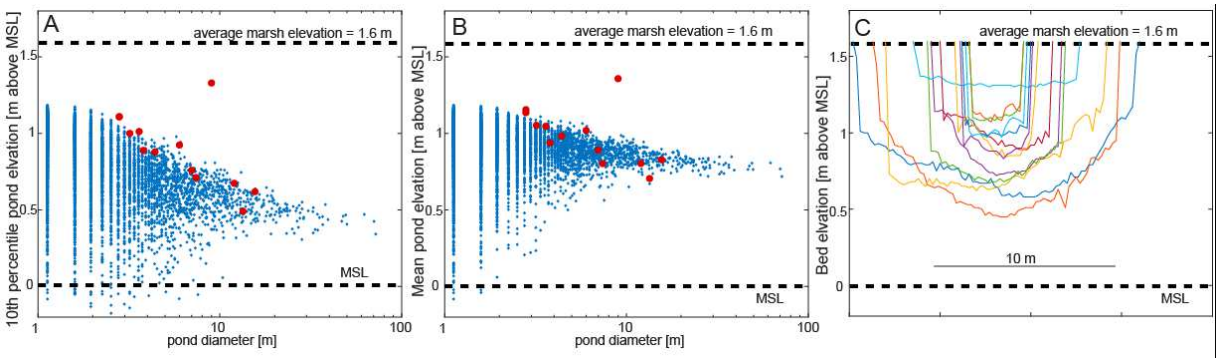

923

924

925 Figure 9

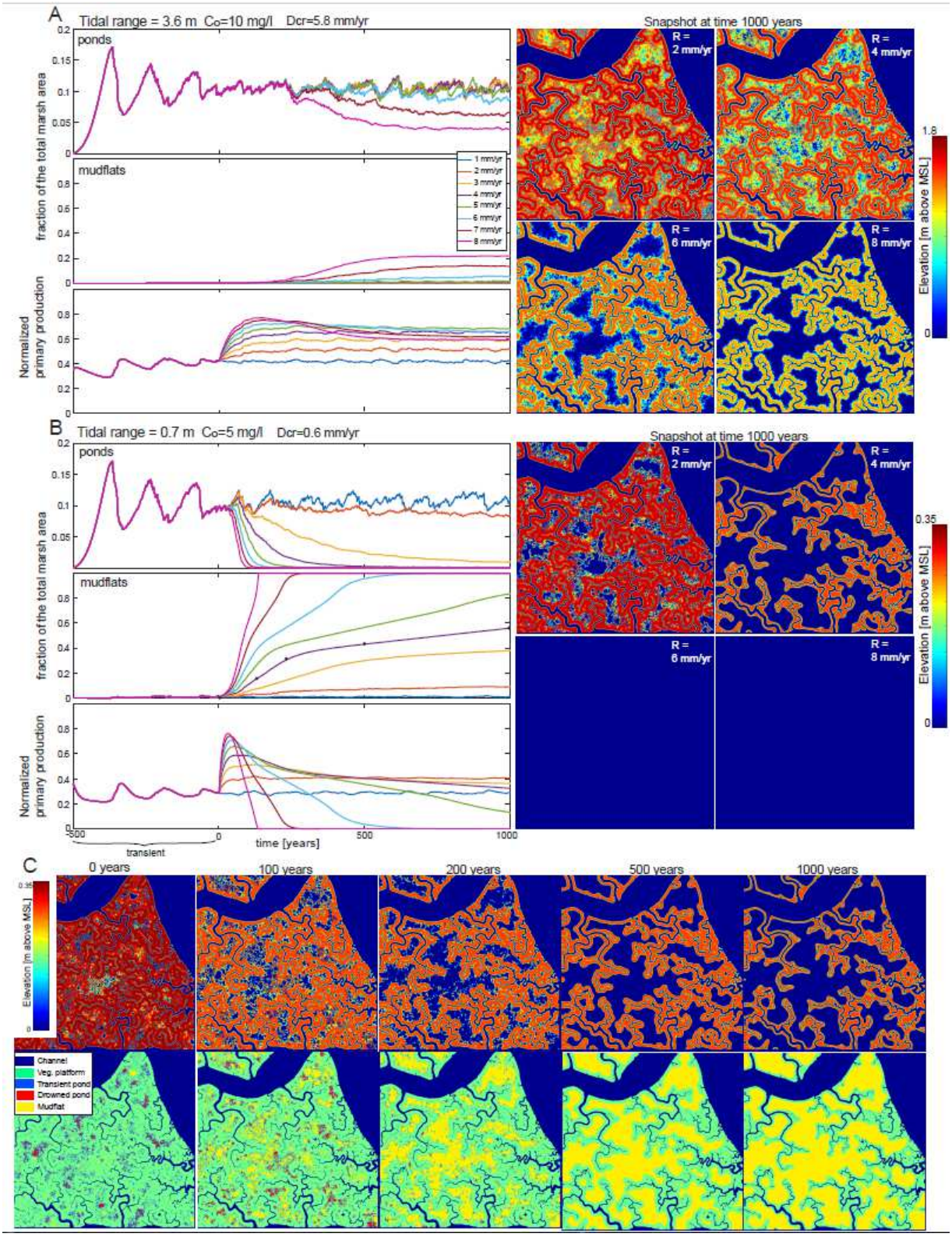

926

927 Figure 10

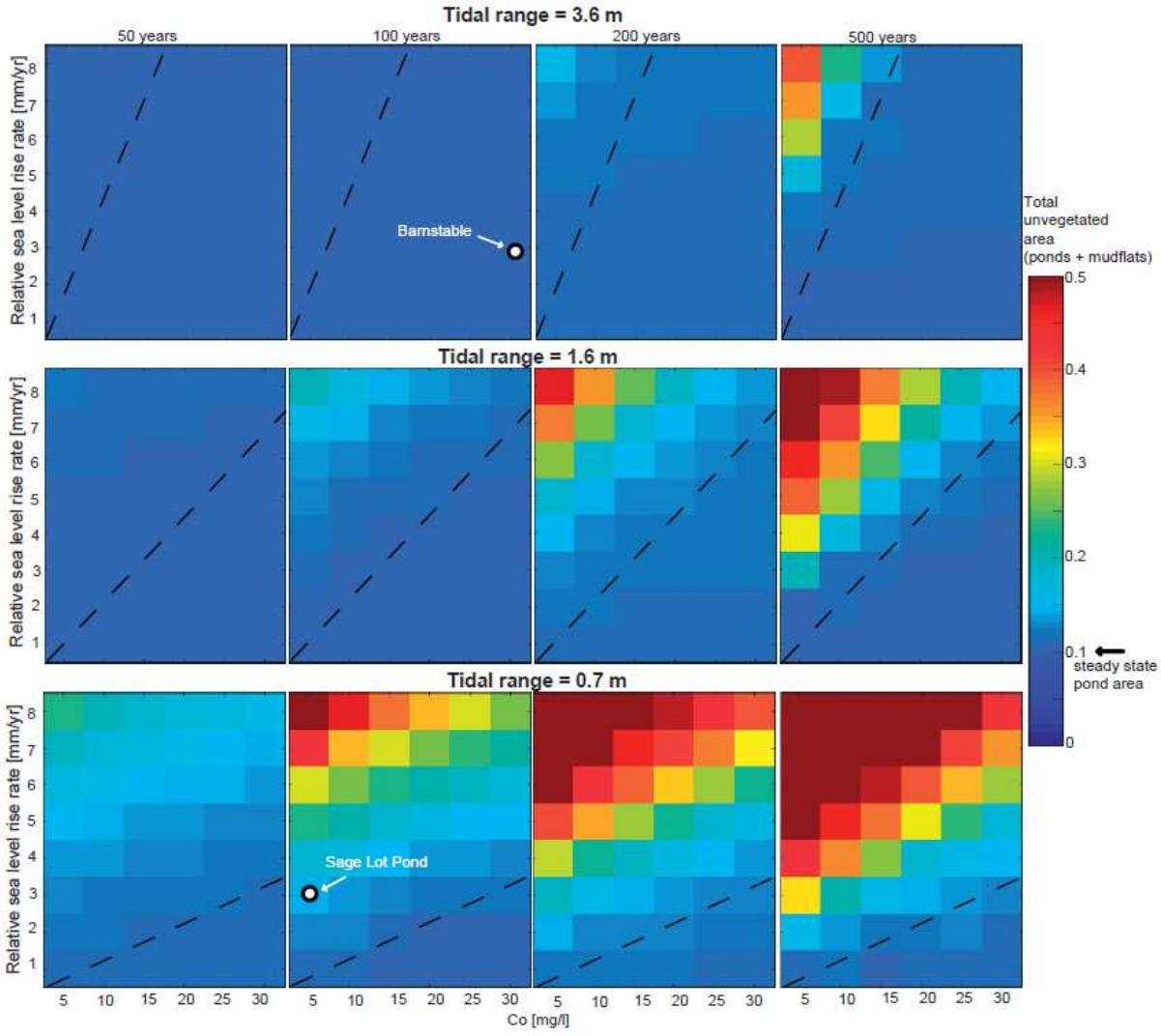

928

929

930

931 Table 1.

Site	Sediment accretion rate (1900 to 2018)
Sage Lot Pond	
Interior (1 core, 13 intervals)	1.4 ± 0.3 mm/yr
Channel-adjacent (1 core, 27 intervals)	3.6 ± 2.0 mm/yr
Barnstable	
Interior (3 cores, 134 intervals)	5.1 ± 3.3 mm/yr
Channel-adjacent (3 cores, 130 intervals)	4.6 ± 2.5 mm/yr

932

933

934

935 Table 2.

Symbol	Description	Value	Reference
Δx	Spatial discretization	1 m	
Δt	Temporal discretization	1 year	
C_o	SSC in channels	30 mg/l or 5 mg/l	Measured
ρ_m	Mud dry bulk density	650 kg/m^3	Assumed
β	Horizontal decay rate of SSC with distance from channel network	0.05 m^{-1}	(Christiansen et al., 2000)
α	Fraction of spatially uniform SSC	0.3	Assumed
r	Spring tidal range	3.6 m or 0.7 m	NOAA Stations 8447930 & 8447241
Δr	Spring-neap variability	0.05r	
T	Tidal period	12.5 hr	
R	Relative Sea Level Rise rate	2.9 mm/yr	
μ	Soil creep diffusivity	0.1 m^2/yr	(Mariotti et al., 2019)
z_{min}	Min elevation for vegetation	0	Assumed
z_{max}	Max elevation for vegetation	r/2	Assumed
D_{pMAX}	Max in-situ organic deposition	6 mm/yr	Assumed
k_{seed}	Pond formation rate	$4 \cdot 10^{-4}$ #ponds/m^2/yr	Calibrated
k_{exp}	Pond expansion rate	0.015 m/yr	Measured
L	Drainage influence length	20 m	Measured
Y_{pond}	Max initial depth of new ponds	$0.25(z_{max}-z_{max})$	Calibrated
$P_{deepening}$	Active deepening of ponds	3 mm/yr	Calibrated

936

937